Metal−Metal Cooperativity Effects in Promoting C−H Bond Cleavage of a Methyl Group by an Adjacent Metal Center

Jeffrey R. Torkelson,[‡] Frederick H. Antwi-Nsiah,[‡] Robert McDonald,[†,‡] Martin Cowie,*[,‡] Justin G. Pruis,[§] Karl J. Jalkanen,[§] and Roger L. DeKock[§]

Contribution from the Department of Chemistry, University of Alberta, Edmonton, AB, Canada T6G 2G2, and Department of Chemistry and Biochemistry, Calvin College, Grand Rapids, Michigan 49546-4388

Received October 5, 1998

Abstract: The reaction of $[Ir_2(CO)_3(dppm)_2]$ (dppm = $Ph_2PCH_2PPh_2$) with methyl triflate yields the methylene-bridged hydride $[Ir_2H(CO)_3(\mu\text{-}CH_2)(dppm)_2][CF_3SO_3]$ (**2**), in which the hydride and methylene hydrogens are rapidly scrambling at ambient temperature. Under CO this species yields the methyl and acyl products $[Ir_2(R)(CO)_4(dppm)_2][CF_3SO_3]$ (R = CH_3, $C(O)CH_3$). Removal of one carbonyl from **2** yields the fluxional methyl complex $[Ir_2(CH_3)(CO)_2(dppm)_2][CF_3SO_3]$ (**3**) in which the methyl group readily migrates from metal to metal. Addition of CO, PR_3, CN^tBu or SO_2 to **3** results in C−H bond cleavage of the methyl group yielding the methylene-bridged, hydride species, $[Ir_2H(CO)_2L(\mu\text{-}CH_2)(dppm)_2][CF_3SO_3]$ (L = CO, PR_3, CN^tBu) or $[Ir_2H(CO)_2(\mu\text{-}CH_2)(\mu\text{-}SO_2)(dppm)_2][CF_3SO_3]$ (**11**). Both the carbonyl and SO_2 adducts are fluxional, having the hydrogens of the hydrido ligand and the methylene group exchanging rapidly at ambient temperature. The activation parameters for this reversible C−H bond-making and -breaking step have been determined ($\Delta H^‡$ = 10.3 kcal/mol, $\Delta S^‡ = -11.2$ cal/mol K (CO); $\Delta H^‡ = 6.1$ kcal/mol, $\Delta S^‡ = -6.2$ cal/mol K (SO_2)). X-ray structure determinations of compound **3**, $[Ir_2H(CO)_2(PMe_3)(\mu\text{-}CH_2)(dppm)_2][CF_3SO_3]$ (**6**), and compound **11** have been determined to confirm the proposed structures. Density functional theory calculations have been carried out on cations related to **3** and **11** by substitution of the phenyl substituents on the dppm ligands by hydrogens, and on key isomers of these, to gain an understanding of the factors promoting C−H bond cleavage in this system. A proposal is presented rationalizing the facile C−H bond cleavage in **3** upon addition of the substrate molecules, in which the roles of the adjacent metals are described.

Introduction

As pointed out by Earl Muetterties more than 15 years ago,[1] "Surface chemistry is coordination chemistry. If the molecule or molecules in question are organic then the surface chemistry is organometallic chemistry." We therefore expect that organic transformations occurring on metal surfaces will be fundamentally no different than those occurring with homogeneous metal complexes. With these parallels in mind, it is therefore not surprising that homogeneous, organometallic complexes can serve as useful models for heterogeneous catalysts in organic transformations.[2] Although heterogeneous systems are notoriously difficult to study, homogeneous systems are more amenable, with the aid of a battery of spectroscopic techniques. The simplest model systems are based on single-metal (mononuclear) complexes; however, one aspect that distinguishes metal surfaces from mononuclear systems is the presence of adjacent metals in the former, which may have a significant effect on the chemistry of interest. The influence of an adjacent metal is clearly indicated in a comparison of alkyl complexes of mononuclear systems and those of clusters. In mononuclear late-metal systems β-hydrogen elimination is common,[3] whereas analogous clusters of two or more metals often give rise to α-hydrogen elimination.[4,5] This difference is readily rationalized upon consideration of the geometries of both systems. In a mononuclear complex, represented by structure **A**, the β-hydrogens are favorably disposed for formation of an agostic interaction[6] with the metal, often leading to C−H bond cleavage.

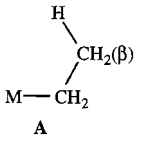

A

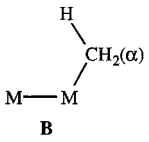

B

In clusters, in which the alkyl group is bound to one metal while adjacent to at least one additional metal, as represented by **B**, the α-hydrogens are oriented so that favorable interactions with the *adjacent* metal can occur,[7] leading to activation of this C−H bond.

Our current interest in binuclear complexes is aimed at determining how adjacent metals can influence the reactivity

* To whom correspondence should be addressed.
‡ University of Alberta.
† Faculty Service Officer, Structure Determination Laboratory.
§ Calvin College.

(1) Muetterties, E. L. *Pure Appl. Chem.* **1982**, *54*, 83.
(2) See for example: (a) Marks, T. J. *Acc. Chem. Res.* **1992**, *25*, 57. (b) Zaera, F. *Chem. Rev.* **1995**, *95*, 2651. (c) Atwood, J. D. *Coord. Chem. Rev.* **1988**, *83*, 93.
(3) Collman, J. P.; Hegedus, L. S.; Norton, J. R.; Finke, R. G. *Principles and Applications of Organotransition Metal Chemistry*; University Science Books: Mill Valley, CA, 1987; p 383.
(4) Crabtree, R. H. *The Organometallic Chemistry of the Transition Metals*; John Wiley & Sons: New York, 1988; p 327.
(5) Calvert, R. B.; Shapley, J. R. *J. Am. Chem. Soc.* **1977**, *99*, 5225.
(6) (a) Brookhart, M.; Green, M. L. H. *J. Organomet. Chem.* **1983**, *250*, 395. (b) Brookhart, M.; Green, M. L. H.; Wong, L.-L. *Prog. Inorg. Chem.* **1988**, *36*, 1.
(7) See for example: Jeffrey, J. C.; Orpen, A. G.; Stone, F. G. A.; Went, M. J. *J. Chem. Soc., Dalton Trans.* **1986**, 173.

10.1021/ja983525o CCC: $18.00
Published on Web 04/06/1999

of catalytically relevant molecules, with a view toward modeling substrate activation by adjacent metals in heterogeneous systems. We begin by considering one of the simplest multinuclear organometallic systems, the binuclear methyl complex. In such complexes the methyl group is capable of displaying several coordination modes.[8] For late-metal systems, three arrangements are possible as diagrammed below. In **C** the methyl group is

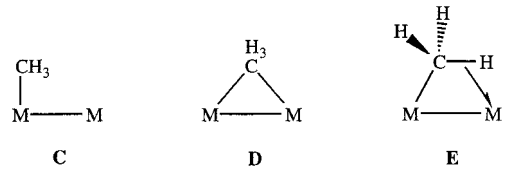

C **D** **E**

terminally bound to one metal and to a first approximation resembles a mononuclear alkyl species. When methyl groups bridge two late metals, two binding modes have been identified. In structure **D** the methyl group bridges the metals symmetrically, giving rise to a three-center metal−carbon−metal interaction,[9] whereas in structure **E**, the methyl group bridges in an unsymmetrical manner, η^1 bound to one metal via carbon and η^2 bound to the adjacent metal via a C−H bond.[10] This latter agostic interaction has important implications relating to the activation of the C−H bond, as noted earlier. In this article we attempt to determine the factors influencing the coordination modes of methyl groups in a binuclear Ir complex, with emphasis on factors leading to C−H bond activation.

Experimental Section

General Comments. All solvents were dried (using appropriate drying agents), distilled before use, and stored under nitrogen. Deuterated solvents used for NMR experiments were degassed and stored under argon over molecular sieves. Reactions were carried out at room temperature (unless otherwise stated) using standard Schlenk procedures, and compounds, which were isolated as solids, were purified by recrystallization. A flow rate of ca. 0.2 mL s^{-1} was used for all reactions that involved purging a solution with a gas. Prepurified argon and hydrogen were purchased from Linde, carbon monoxide and sulfur dioxide were purchased from Matheson, and carbon-13-enriched CO (99%) was supplied by Isotec Inc. All gases were used as received. Ammonium hexachloroiridate(IV) was purchased from Vancouver Island Precious Metals, and the chemicals, methyl triflate, d^3-methyl triflate, ^{13}C-methyl triflate, *tert*-butyl isocyanide, 2,3,6,6-tetramethylpiperidine, all phosphines, and triphenyl phosphite were purchased from Aldrich. The compound $[Ir_2(CO)_3(dppm)_2]$ (**1**) was prepared as previously reported.[11]

Standard NMR spectra were recorded on a Bruker AM-400 spectrometer operating at 400.1 MHz for ^{1}H, 161.9 MHz for ^{31}P, and 100.6 MHz for ^{13}C spectra. The solid-state $^{13}C\{^1H\}$ NMR spectrum was recorded on a Bruker AMR-300 spectrometer [with a magic-angle spinning (MAS) accessory] operating at 75.5 MHz. The $^{13}C\{^1H\}\{^{31}P\}$ NMR spectra were obtained on a Bruker WH-200 spectrometer operating at 50.3 MHz. All ^{13}C NMR spectra were obtained using ^{13}CO- or $^{13}CH_3$-enriched samples (the latter obtained from ^{13}C-methyl triflate). Infrared spectra were obtained on a Nicolet 7199 Fourier transform interferometer, either as solids in Nujol, as CH_2Cl_2 casts on KBr plates, or as solutions in KCl cells with 0.5-mm-window path lengths. Carbonyl stretches reported are for isotopically nonenriched samples. The elemental analyses were performed by the microanalytical service within the department. Spectroscopic data for all compounds are given in Table 1.

Preparation of Compounds. (a) $[Ir_2(H)(CO)_3(\mu\text{-}CH_2)(dppm)_2][CF_3SO_3]$ (2). The compound $[Ir_2(CO)_3(dppm)_2]$ (**1**) (100 mg, 0.081 mmol) was dissolved in 10 mL of benzene, to which was added 1 equiv of methyl triflate (9.1 μL, 0.081 mmol). The light yellow solution immediately darkened to orange and turned cloudy after about 10 min. The mixture was stirred for 3 h by which time a yellow precipitate had formed. Removal of the solvent under vacuum gave a yellow product which was recrystallized from CH_2Cl_2/Et_2O. This solid was dried under a stream of argon and put under vacuum for about 18 h, during which time the color changed from yellow to light brown (86% yield). Anal. Calcd for $Ir_2SP_4F_3O_6C_{55}H_{47}$: C, 47.20; H, 3.37. Found: C, 47.32; H, 3.40.

(b) $[Ir_2(CH_3)(CO)(\mu\text{-}CO)(dppm)_2][CF_3SO_3]$ (3). Compound **2** (80 mg, 0.057 mmol) was dissolved in 5 mL of CH_2Cl_2. One equivalent of anhydrous Me_3NO (4.3 mg, 0.057 mmol), dissolved in 5 mL of CH_2Cl_2, was added dropwise from an addition funnel to the solution of **2** during 15 min, while maintaining a slow stream of argon over the solution. The mixture was stirred for 45 min, resulting in a color change to dark red, and the solvent was removed under vacuum. The solid was then recrystallized from CH_2Cl_2/Et_2O, dried under argon, and then in vacuo (78% yield). Anal. Calcd for $Ir_2SP_4F_3O_5C_{54}H_{47}$: C, 47.23; H, 3.45. Found: C, 46.81; H, 3.24.

(c) $[Ir_2(H)(CO)_2(PMe_3)(\mu\text{-}CH_2)(dppm)_2][CF_3SO_3]$ (6). Method A. A solution of PMe_3 [71.4 μL of a 1 M solution in tetrahydrofuran (THF) (0.071 mmol)] in 10 mL of THF was added to a 20-mL THF solution of compound **2** (100 mg, 0.071 mmol), resulting in an immediate color change from orange to bright yellow. The solution was stirred for 2 h during which time a yellow precipitate formed. Removal of the solvent under vacuum gave a light yellow microcrystalline solid, which was then recrystallized from THF/Et_2O (70% yield).

Method B. To a solution of compound **3** (30 mg, 0.022 mol) in 0.6 mL of CD_2Cl_2, in an NMR tube capped with a rubber septum, was added 1 equiv (2.3 μL, 0.022 mmol) of PMe_3 leading to an immediate color change to bright yellow. The NMR spectra showed that the product was compound **6**. Anal. Calcd for $Ir_2SP_5F_3O_5C_{57}H_{56}$: C, 47.23; H, 3.89. Found: C, 47.12; H, 4.12.

(d) $[Ir_2(H)(CO)_2(PMe_2Ph)(\mu\text{-}CH_2)(dppm)_2][CF_3SO_3]$ (7). Method A. The procedure was the same as that described for compound **6** except that PMe_2Ph (99%) was used instead of a 1 M THF solution of PMe_3 (67% yield).

Method B. To a solution of compound **3** (30 mg, 0.022 mmol) in 0.6 mL of CD_2Cl_2, in an NMR tube capped with a rubber septum, was added 1 equiv (3.1 μL, 0.022 mmol) of PMe_2Ph leading to an immediate color change to yellow. The NMR spectra showed that the product was compound **8**. Anal. Calcd for $Ir_2SP_5F_3O_5C_{62}H_{58}$: C, 49.27; H, 3.87. Found: C, 49.08; H, 3.71.

(e) $[Ir_2(H)(CO)_2(PPh_3)(\mu\text{-}CH_2)(dppm)_2][CF_3SO_3]$ (8). Method A. Compound **2** (100 mg, 0.071 mmol) was dissolved in 20 mL of THF, to which was added 1 equiv of PPh_3 (19 mg, 0.071 mmol) dissolved in 10 mL of THF. The solution color changed from orange to yellow. After stirring for 2 h, the solvent was removed under vacuum, and the yellow solid recrystallized from CH_2Cl_2/Et_2O.

Method B. Compound **3** (20 mg, 0.015 mmol) and PPh_3 (4.3 mg, 0.016 mmol) were placed in an NMR tube to which 0.6 mL of CD_2Cl_2 was added resulting in an immediate color change to orange. The NMR spectra showed that the product was compound **7**.

(f) $[Ir_2(H)(CO)_2(P(OPh)_3)(\mu\text{-}CH_2)(dppm)_2][CF_3SO_3]$ (9a and 9b). The procedure was the same as that described for **6** except that $P(OPh)_3$ (97%) was used instead of a 1 M THF solution of PMe_3, and the mixture was stirred for 3 h instead of 2 h. Two isomers were formed (see Results and Characterization) (60% total yield). Anal. Calcd for $Ir_2SP_5F_3O_8C_{72}H_{62}$: C, 51.36; H, 3.71. Found: C, 51.40; H, 3.82.

(g) $[Ir_2(H)(CO)_2(^tBuNC)(\mu\text{-}CH_2)(dppm)_2][CF_3SO_3]$ (10). Method A. To a solution of compound **2** (100 mg, 0.071 mmol) in 5 mL of CH_2Cl_2, was added 1 equiv of ^{t}BuNC (8.1 μL, 0.071 mmol), causing an immediate color change from orange to yellow. The mixture was

(8) See for example: Schwartz, D. J.; Ball, G. E.; Andersen, R. A. *J. Am. Chem. Soc.* **1995**, *117*, 6027.

(9) See for example: (a) Schmidt, G. F.; Muetterties, E. L.; Beno, M. A.; Williams, J. M. *Proc. Natl. Acad. Sci. U.S.A.* **1981**, *78*, 1318. (b) Kulzick, M. A.; Price, R. T.; Andersen, R. A.; Muetterties, E. L. *J. Organomet. Chem.* **1987**, *333*, 105. (c) Reinking, M. K.; Fanwick, P. E.; Kubiak, C. P. *Angew. Chem., Int. Ed. Engl.* **1989**, *28*, 1377.

(10) See for example: (a) Dawkins, G. M.; Green, M.; Orpen, A. G.; Stone, F. G. A. *J. Chem. Soc. Chem. Commun.* **1982**, 41. (b) Calvert, R. B.; Shapley, J. R. *J. Am. Chem. Soc.* **1978**, *100*, 7726. (c) Brookhart, M.; Green, M. L. H.; Wong, L.-L. *Prog. Inorg. Chem.* **1988**, *36*, 1; and references therein.

(11) Sutherland, B. R.; Cowie, M. *Organometallics* **1985**, *4*, 1637.

Table 1. Spectroscopic Data for the Compounds

compound[a,b]	$\delta(^{31}P\{^1H\})$[c]	$\delta(^1H)$[d,e]	$\delta(^{13}C\{^1H\})$[d]	IR, cm^{-1} [f,g]
$[Ir_2(H)(CO)_3(\mu\text{-}CH_2)(dppm)_2][CF_3SO_3]$ (**2**)[h]	−0.9(m), −12.5(m)	5.19 (m, 2H), 4.60 (m, 2H), 3.59 (m, $^1J_{C-H}$ = 140.6 Hz, 2H),[c] −11.35 (t, 1H)	177.4(t, 1C), 177.0 (t, 1C), 162.0 (t, 1C), 49.4 (b, 1C)	2018 (vs), 2000 (vs), 1970 (vs)
$[Ir_2(CH_3)(CO)_2(dppm)_2][CF_3SO_3]$ (**3**)	22.1(s)	4.45 (m, 2H), 3.79 (m, 2H), 0.58 (q, $^3J_{P-H}$ = 4.1 Hz, 3H, $^1J_{C-H}$ = 127 Hz)[j]	171.4 (b, 2C), 17.5 (q, $^2J_{C-P}$ = 3.9 Hz, 1C)	1964 (s),[i] 1886 (w)
			187.8 (m, 1C),[k] 167.0 (m, 1C)[k]	1974 (vs), 1832 (s)
$[Ir_2(CH_3)(CO)_4(dppm)_2][CF_3SO_3]$ (**4**)	−8.9(m), −16.0(m)	4.59 (m, 4H), 0.38 (t, 3H)	194.2 (t, 2C), 182.9 (t, 2C)	2038 (m),[i] 1977 (b, vs), 1956 (vs)
$[Ir_2(COCH_3)(CO)_4(dppm)_2][CF_3SO_3]$ (**5**)	−9.6(m), −25.5(m)	4.61 (b, 4H), 0.63 (s, 3H)	225.1 (t, 1C), 195.6 (b, 2C), 179.9 (t, 2C)	2019 (m),[i] 1988 (sh), 1959 (s), 1622 (w)
$[Ir_2(H)(CO)_2(PMe_3)(\mu\text{-}CH_2)(dppm)_2][CF_3SO_3]$ (**6**)	−7.7(m), −11.3(m), −79.2(b)	4.05 (m, 2H), 3.45 (m, 2H), 3.05 (m, 2H), 0.75 (d, 9H), −12.35 (dm, $^3J_{P-H}$ = 21.1, 4.8, $^2J_{P-H}$ = 13.5 Hz, 1H)	183.0 (t, 1C), 180.1 (b, 1C)	1961 (vs), 1950 (vs)
$[Ir_2(H)(CO)_2(PMe_2Ph)(\mu\text{-}CH_2)(dppm)_2][CF_3SO_3$ (**7**)	5.7(m), −12.1(m), −71.6(b)	3.82 (m, 2H), 3.35 (m, 2H), 3.30 (m, 2H), 1.12 (d, 6H), −12.2 (dm, $^3J_{P-H}$ = 21.6 Hz, 1H)	182.6 (t, 1C), 180.6 (b, 1C)	1963 (vs), 1952 (s)
$[Ir_2(H)(CO)_2(PPh_3)(\mu\text{-}CH_2)(dppm)_2][CF_3SO_3]$ (**8**)	−4.1(m), −13.7(m), −33.9(b)	3.84 (m, 2H), 3.71 (m, 2H), 3.13 (M, 2H), −13.25 (dm, $^3J_{P-H}$ = 22.3 Hz, 1H)	183.4 (t, 1C), 180.5 (b, 1C)	1975 (vs), 1948 (vs)
$[Ir_2(H)(CO)_2(P(OPh)_3)(\mu\text{-}CH_2)(dppm)_2][CF_3SO_3]$ (**9a**)	43.9(m), −4.1(m), −12.6(m)	5.2−3.7 (m), −12.69 (dm, $^3J_{P-H}$ = 37.3 Hz, 1H)	180.4 (b, 1C), 179.7 (t, 1C), 167.1 (dt, 1C)	1985 (vs), 1975 (vs), 1951 (s)
$[Ir_2(H)(CO)_2(P(OPh)_3)(\mu\text{-}CH_2)(dppm)_2][CF_3SO_3]$ (**9b**)	82.7(t), −5.6(m), −8.1(m)	5.2−3.7 (m), −11.71 dt, $^2J_{P-H}$ = 17.7 Hz, 1H)		
$[Ir_2(H)(CO)_2(CN^tBu)(\mu\text{-}CH_2)(dppm)_2][CF_3SO_3]$ (**10**)	−6.6(m), −8.5(m)	3.92 (m, 2H), 3.58 (m, 2H), 3.57 (m, 2H), 0.60 (s, 9H), −11.46 (t, 1H)	179.2 (b, 1C), 179.1 (t, 1C)	2163 (s),[l] 1975 (s), 1970 (s)
$[Ir_2(H)(CO)_2(\mu\text{-}CH_2)(\mu\text{-}SO_2)(dppm)_2][CF_3SO_3]$ (**11**)	−1.0(s)	4.50 (m, 2H), 3.94 (m, 2H), −2.15 (b, $^1J_{C-H}$ = 98 Hz, 3H)[j]	170.8 (t, 2C), 36.1 (q, $^2J_{C-P}$ = 4.5 Hz, 1C)	2044 (vs), 1997 (vs)
$[Ir_2(CH_3)(CO)_3(\mu\text{-}SO_2)(dppm)_2][CF_3SO_3]$ (**12**)	−0.4(m), −14.7(m)	4.9 (m, 2H), 3.40 (m, 2H), 0.01 (t, 3H)	177.9 (t, 1C), 177.8 (t, 1C), 160.2 (t, 1C)	2042 (s), 2010 (vs), 1987 (s), 1070 (m)[m]
$[Ir_2(CH_3CO)(CO)_3(\mu\text{-}SO_2)(dppm)_2][CF_3SO_3]$ (**13**)	−5.0(m), −13.8(m)	5.03 (m, 2H), 3.18 (m, 2H), 1.28 (s, 3H)		2013 (s), 1990 (vs), 1646 (m)

[a] NMR abbreviations: s = singlet, d = doublet, t = triplet, m = multiplet, q = quintet, dm = doublet of multiplets, b = broad. [b] NMR data at 25 °C in CD_2Cl_2 unless otherwise stated. [c] $^{31}P\{^1H\}$ chemical shifts are referenced vs external 85% H_3PO_4. [d] ^1H and ^{13}C vs external TMS. [e] Chemical shifts for the phenyl hydrogens are not given in the ^1H NMR data. [f] IR abbreviations [ν(CO) unless otherwise stated]: vs = very strong, s = strong, m = medium, w = weak, sh = shoulder, b = broad. [g] Nujol mull or CH_2Cl_2 cast unless otherwise stated. [h] Data at −40 °C. [i] CH_2Cl_2 solution. [j] $^1J_{C-H}$ coupling values for ^{13}C-labeled compounds. [k] Solid-state NMR. [l] ν(CN). [m] ν(SO).

Table 2. Crystallographic Data

compd	$[Ir_2(CH_3)(CO)(\mu\text{-}CO)(dppm)_2][CF_3SO_3]$ (**3**)	$[Ir_2(H)(PMe_3)(CO)_2(\mu\text{-}CH_2)(dppm)_2]$-$[CF_3SO_3]\cdot 2CH_2Cl_2$ (**6**)	$[Ir_2(H)(CO)_2(\mu\text{-}CH_2)(\mu\text{-}SO_2)(dppm)_2]$-$[CF_3SO_3]\cdot CH_2Cl_2$ (**11**)[a]
formula	$C_{54}H_{47}F_3Ir_2O_5P_4S$	$C_{59}H_{60}Cl_4F_3Ir_2O_5P_5S$	$C_{54.875}H_{48.625}Cl_{2.125}F_3Ir_2O_7P_4S_2$[a]
formula wt	1373.26	1619.18	1524.79
color	dark red	yellow	dark red
crystal system	monoclinic	triclinic	monoclinic
space group	$P2_1/n$ (an alternate setting of $P2_1/c$ [No. 14])	$P\bar{1}$ (No. 2)	$P2_1/c$ (No. 14)
unit cell parameters			
a (Å)	13.8372 (14)	11.910 (2)	13.974 (2)
b (Å)	15.569 (2)	12.8934 (15)	18.422 (3)
c (Å)	23.629 (2)	20.532 (3)	22.264 (3)
α (deg)	90.0	91.256 (10)	90.0
β (deg)	96.413 (9)	95.308 (13)	105.25 (1)
γ (deg)	90.0	102.601 (12)	90.0
V (Å$^{3)}$	5058.5 (10)	3060.9 (8)	5532.6 (12)
Z	4	2	4
R[b] $[F_o^2 > 2\sigma(F_o^2)]$	0.0405	0.0598	0.0505
wR_2[b] $[F_o^2 > -3\sigma(F_o^2)]$	0.0815	0.1798	0.1298
GOF(S)[c]	$1.003[F_o^2 \geq -3\sigma(F_o^2)]$	$1.082[F_o^2 \geq -3\sigma(F_o^2)]$	$0.993[F_o^2 \geq -3\sigma(F_o^2)]$

[a] Compound **11** cocrystallized with 12.5% $[Ir_2(CO)_2(\mu\text{-}Cl)(\mu\text{-}SO_2)(dppm)_2][CF_3SO_3]\cdot CH_2Cl_2$. [b] $R_1 = \sum||F_o| - |F_c||/\sum|F_o|$; $wR_2 = [\sum w(F_o^2 - F_c^2)^2/\sum w(F_o^4)]^{1/2}$. [c] $S = [\sum w(F_o^2 - F_c^2)^2/(n-p)]^{1/2}$ (n = number of data; p = number of parameters varied; $w = [\sigma^2(F_o^2) + (a_0P)^2 + a_1P]^{-1}$, where $P = [\mathrm{Max}(F_o^2, 0) + 2F_c^2]/3$), and a_0 and a_1 are suggested by the least-squares program for each structure (for **3**, $a_0 = 0.0216$, $a_1 = 2.2944$; for **6**, $a_0 = 0.1278$, $a_1 = 10.1840$; for **11**, $a_0 = 0.0554$, $a_1 = 0$).

stirred for 2 h by which time the color was green. The solvent volume was reduced to about 2 mL, and the green product was precipitated and washed with Et_2O. After drying under an argon stream, the solid was recrystallized from CH_2Cl_2/Et_2O (70% yield).

Method B. Compound **3** was substituted for compound **2** in the above-mentioned procedure yielding compound **10** essentially quantitatively (by NMR).

Elemental analyses for compound **10** always gave low values for %C and %H because of decomposition in air.

(h) $[Ir_2(H)(CO)_2(\mu\text{-}CH_2)(\mu\text{-}SO_2)(dppm)_2][CF_3SO_3]$ (11). Sulfur dioxide gas was passed through a solution of compound **3** (60 mg, 0.044 mmol) in 5 mL of CH_2Cl_2 for 1 min, leading to an immediate color change of the solution from red to dark red. After stirring for 10 min, the solution was concentrated to about 2 mL under an argon stream and the dark red-brown solid was precipitated and washed twice with Et_2O. The solid was dried under an argon stream and then under vacuum (72% yield). Anal. Calcd for $Ir_2S_2P_4F_3O_7C_{54}H_{47}$: C, 45.12; H, 3.30; S, 4.46. Found: C, 45.40; H, 3.16; S, 4.19.

(i) $[Ir_2(CH_3)(CO)_3(\mu\text{-}SO_2)(dppm)_2][CF_3SO_3]$ (12). Sulfur dioxide gas was passed through a solution of **3** (30 mg, 0.022 mmol) in 5 mL of CH_2Cl_2 for about 2 min, resulting in a color change from red to dark red indicating the formation of **11**. CO was then passed through the solution for 5 min and the color changed from dark red to light yellow, then to green. The solution was stirred under a static atmosphere of the gas for 15 min, after which time the green solid was precipitated with Et_2O. The solid was collected, washed with Et_2O and dried under an argon stream. It was then recrystallized from CH_2Cl_2/Et_2O (73% yield). Anal. Calcd. for $Ir_2S_2P_4F_3O_8C_{55}H_{47}$: C, 45.19; H, 3.23; S, 4.37. Found: C, 44.54; H, 3.21; S, 4.77.

(j) Reaction of Compound 3 with CO. To a solution of compound **3** (30 mg, 0.022 mmol) in 0.6 mL of CD_2Cl_2, in an NMR tube capped with a rubber septum, was added 2 mL of CO, by means of a gas-tight syringe, leading to an immediate color change from red to yellow. The NMR spectra showed that the reaction mixture contained $[Ir_2(CH_3)(CO)_4(dppm)_2][CF_3SO_3]$ (**4**) and $[Ir_2(COCH_3)(CO)_4(dppm)_2][CF_3SO_3]$ (**5**) in a typical ratio of about 1.0:0.2. However, the products were not isolated as solids, because they are unstable in the absence of a CO atmosphere.

(k) Reaction of Compound 12 with CO. The procedure was the same as the reaction of compound **3** with CO. The NMR spectrum of the reaction mixture showed that it contained unreacted compound **12** and $[Ir_2(CH_3CO)(CO)_3(\mu\text{-}SO_2)(dppm)_2][CF_3SO_3]$ (**13**), in a typical ratio of 3:1. However the acyl product was not isolated as a solid, because it reverted to **12** in the absence of a CO atmosphere.

^{1}H NMR Magnetization Transfer Experiments on Compound 2. Magnetization transfer between the hydride and the methylene-ligand protons was examined by selective inversion. The hydride signal was selectively inverted by means of a DANTE[12] pulse sequence. Typically, after a delay of 1.5 s, a series of eighteen 5-μs pulses, each separated by a 550-μs delay was used. The relaxation of this signal after the inversion was monitored using a 90° nonselective observation pulse, applied at variable delays of between 0.001 and 2.5 s, after the selective pulse.

Nonselective inversion recovery experiments were performed initially to measure the relaxation time (T_1) for the hydride as well as that for the methylene ligand protons. The nonselective 90° pulse width for ^{1}H, with an attenuator set at 10 dB, was 44.75 μs. This pulse width was calibrated at the beginning of the experiment. NMR probe temperatures were measured with an independently calibrated thermocouple immersed in the appropriate volume of toluene in an NMR tube before and after the experiments.

X-ray Data Collection. For each of compounds **3**, **6**, and **11**, crystals suitable for X-ray diffraction were grown via slow diffusion of diethyl ether into a concentrated CH_2Cl_2 solution of the compound. Crystals were mounted and flame-sealed in glass capillaries under solvent vapor to minimize decomposition or deterioration caused by solvent loss. Data were collected at −50 °C on an Enraf-Nonius CAD4 diffractometer using graphite-monochromated Mo Kα radiation. Unit cell parameters and space group assignments were obtained as described below. For each compound, three reflections were chosen as intensity standards and were remeasured every 120 min of X-ray exposure time; in no case was decay evident. Absorption corrections were applied to the data as described below. Crystal parameters and final agreement factors are summarized in Table 2.

Unit cell parameters for compounds **3**, **6**, and **11** were obtained from a least-squares refinement of 24 reflections in the approximate range $20° < 2\theta < 24°$. For compounds **3** and **11** the cell parameters and the systematic absences defined the space groups as $P2_1/n$ and $P2_1/c$, respectively, whereas for **6** the cell parameters, the lack of absences, and the diffraction symmetry suggested the space group $P1$ or $P\bar{1}$, the latter of which was established by successful refinement of the structure. Absorption corrections to **3** and **6** were applied by the method of Walker and Stuart,[13] whereas for **11** the crystal faces were indexed and measured, and a Gaussian integration carried out.

(12) Bodenhausen, G.; Freeman, R.; Morris, G. A. *J. Magn. Reson.* **1976**, *23*, 171.

(13) Walker, N.; Stuart, D. *Acta Crystallogr., Sect. A* **1983**, *39*, 158.

Structure Solution and Refinement. For each structure, the positions of the iridium and phosphorus atoms were found using the direct-methods program SHELXS-86,[14] and the remaining atoms were found using a succession of least-squares and difference Fourier maps. Refinement of each structure proceeded using the program SHELXL-93.[15] Hydrogen atom positions (except for hydride ligands as noted below) were calculated by assuming idealized sp^2 or sp^3 geometries about their attached carbon atoms (as appropriate), and were given thermal parameters 120% of the equivalent isotropic displacement parameters of their attached carbons. Further details of structure refinement (other than described below) and final residual indices may be found in Table 2.

For $[Ir_2(CH_3)(CO)(\mu\text{-}CO)(dppm)_2][CF_3SO_3]$ (**3**) electron density maps in the equatorial plane, essentially perpendicular to the Ir−P vectors, indicated similar coordination environments for both iridium atoms. Although the bridging carbonyl group was well behaved, each Ir apparently had a terminal CO in which the peaks corresponding to the oxygens were of low intensity. This suggested a disorder involving superposition of the terminal carbonyl and methyl ligands, resulting from the two orientations of the complex as diagrammed below (dppm groups, above and below the plane of the paper, omitted for clarity).

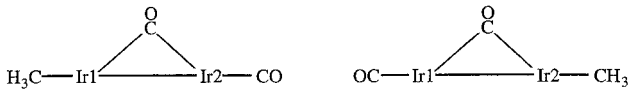

Subsequent difference Fourier maps showed that the disordered carbonyl and methyl carbons were not exactly superimposed but were slightly offset from each other, and these two half-occupancy positions on each Ir refined well. The atoms corresponding to the disordered CO and CH_3 groups were refined isotropically with an occupancy factor of 0.5.

Location of all atoms in $[Ir_2(H)(CO)_2(PMe_3)(\mu\text{-}CH_2)(dppm)_2][CF_3SO_3]\cdot 2CH_2Cl_2$ (**6**) proceeded smoothly, and even the hydride ligand H(2) was located and refined with a fixed Ir(2)−H(2) distance of 1.70 Å.

Although all the nonhydrogen atoms of $[Ir_2(H)(CO)_2(\mu\text{-}CH_2)(\mu\text{-}SO_2)(dppm)_2][CF_3SO_3]\cdot CH_2Cl_2$ (**11**) were located, the carbon atom of the bridging methylene group [C(3)] did not behave well in least-squares refinements. A difference Fourier map at this stage located another peak near C(3), but at approximately 2.5 Å from each metal. A $^{31}P\{^1H\}$ NMR spectrum obtained on a few of the single crystals showed about 10−15% of the previously characterized $[Ir_2(CO)_2(\mu\text{-}Cl)(\mu\text{-}SO_2)(dppm)_2][CF_3SO_3]$,[16] which had apparently resulted from reaction of **11** with the chlorinated solvent. All subsequent attempts to obtain suitable crystals of **11** without the chloro-bridged impurity failed; attempts to grow crystals in nonchlorinated solvents gave poor quality crystals. Inclusion of a chlorine atom [Cl(1)] in the least-squares refinement with an occupancy factor of 0.125 [and concomitant reduction of the occupancy factor for C(3) to 0.875] yielded the most satisfactory results. The hydride ligand H(1) was not located from a difference Fourier map, but its position was idealized at 1.70 Å from Ir(1) in a position that minimized contacts with the surrounding ortho-hydrogen atoms of the dppm groups. Unfortunately, owing to the disorder in which the fractional Cl atom was essentially superimposed on the CH_2 group, the methylene hydrogens could not be located.

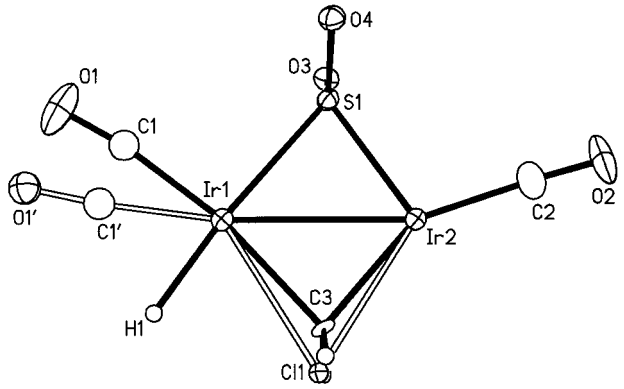

Figure 1. A view of the equatorial plane of compound **11** (87.5% occupancy), showing the disorder involving the superimposed 12.5% occupancy $[Ir_2(CO)_2(\mu\text{-}Cl)(\mu\text{-}SO_2)(dppm)_2]^+$. The major species is shown with solid bonds, whereas the minor species having Cl(1) replacing C(3)H_2 and H(1), and C(1′)O(1′) replacing C(1)O(1) is shown with these changes designated by open bonds.

Disorder of the carbonyl group attached to Ir(1) was suggested by the elongation of the thermal ellipsoids of C(1) and O(1) in a direction perpendicular to the Ir(1)−C(1) bond axis. In addition, the Ir(2)−Ir(1)−C(1) angle observed for **11** (ca. 144°) was substantially different from that previously determined for the chloro-bridged complex (ca. 167°) indicating that these carbonyl groups for the two disordered molecules would not be superimposed. This carbonyl group was therefore disordered over two sites having occupancy factors of 0.875 and 0.125, corresponding to those of the bridging methylene and chloro groups, respectively. The placement of C(1′)O(1′) was initially set at the coordinates previously found for the pure chloro-bridged species, and was refined as a rigid group having Ir(1)−C(1′), C(1′)−O(1′), and Ir(1)−O(1′) distances approximating those within the Ir(2)−C(2)−O(2) unit. Atom C(1′) was given a fixed isotropic thermal parameter roughly equal to U_{eq} for C(2) whereas O(1′) was refined isotropically. Carbonyl C(1)O(1) having the major occupancy was refined anisotropically without restriction. A drawing of the equatorial plane of the disordered structure (dppm groups omitted) is shown in Figure 1. Atoms Ir(1), Ir(2), C(2), O(2), S(1), O(3), and O(4) are common to both disordered molecules and C(1′), O(1′), and Cl(1) corresponding to the chloro-bridged species and C(3)H_2, C(1), O(1), and H(1) belonging to the methylene-bridged complex (**11**). Superposition of the atom positions of complex **11** with the pure chloro-bridged species shows that, apart from the atoms involved in the disorder, all atoms superimpose almost exactly.

Theoretical Methods and Software. We have used the Gaussian 94[17] and Mulliken 2.0.1[18] software suites running on the SGI Indigo II (G94, Rev. D.1) and IBM RS/6000 (G94, Rev. D.2) workstations at Calvin College. Selected Gaussian 94 calculations were performed on the SGI Power Challenge Array at the National Center for Supercomputing Applications (NCSA). Details regarding methodology and basis sets may be found in the Gaussian User's Reference.[19] In Gaussian 94 we used density functional theory (DFT) with the B3LYP methodol-

(14) Sheldrick, G. M. *Acta Crystallogr., Sect. A* **1990**, *46*, 467−473.

(15) Sheldrick, G. M. *SHELXL-93*, program for crystal structure determination; University of Göttingen: Germany, 1993. Refinement on F_o^2 for all reflections except for those having $F_o^2 < -3\sigma(F_o^2)$. Weighted *R*-factors wR_2 and all goodnesses-of-fit *S* are based on F_o^2; conventional *R*-factors R_1 are based on F_o, with F_o set to zero for negative F_o^2. The observed criterion of $F_o^2 > 2\sigma(F_o^2)$ is used only for calculating R_1, and is not relevant to the choice of reflections for refinement. *R*-factors based on F_o^2 are statistically about twice as large as those based on F_o, and *R*-factors based on ALL data will be even larger.

(16) (a) Torkelson, J. R.; Cowie, M. Unpublished results, 1994. (b) Crystal data for $[Ir_2(CO)_2)(\mu\text{-}Cl)(\mu\text{-}SO_2)(dppm)_2][CF_3SO_3]\cdot CH_2Cl_2$: monoclinic; $P2_1/c$; $a = 14.053(3)$ Å, $b = 18.485(4)$ Å, $c = 22.544(6)$ Å, $\beta = 105.89(1)°$; $V = 5633(2)$ Å^3; $Z = 4$; $D_{calc} = 1.819$ g cm^{-3}; μ(Mo Kα) = 51.11 cm^{-1}; $T = 22$ °C; 6489 independent observations $F_o^2 \geq 2\sigma(F_o^2)$; 676 variables; $R_1(F) = 0.0532$ (observed data), $wR_2(F^2) = 0.1273$ (all data).

(17) Frisch, M. J.; Trucks, G. W.; Schlegel, H. B.; Gill, P. M. W.; Johnson, B. G.; Robb, M. A.; Cheeseman, J. R.; Keith, T. A.; Petersson, G. A.; Montgomery, J. A.; Raghavachari, K.; Al-Laham, M. A.; Zakrzewski, V. G.; Ortiz, J. V.; Foresman, J. B.; Cioslowski, J.; Stefanov, B. B.; Nanyakkara, A.; Challacombe, M.; Peng, C. Y.; Ayala, P. Y.; Chen, W.; Wong, M. W.; Andres, J. L.; Replogle, E. S.; Gomperts, R.; Martin, R. L.; Fox, D. J.; Binkley, J. S.; Defrees, D. J.; Baker, J.; Stewart, J. P.; Head-Gordon, M.; Gonzalez, C.; Pople, J. A. *Gaussian 94*, Revisions D.1, D.3, and D.4; Gaussian, Inc.: Pittsburgh, PA, 1995.

(18) Lengsfield, B. H., III; Horn, H.; Swoe, W. C.; Carter, J. T.; McLean, A. D.; Carter, J. T.; Replogle, E. S.; Rice, J. E.; Barnes, L. A.; Maluendes, S. A.; Lie, G. C.; Gutowski, M.; Rudge, W. E.; Sauer, S. P. A.; Lindh, R.; Andersson, K.; Chevalier, T. S.; Widmark, P.-O.; Bouzida, D.; Nesbet, R.; Singh, K.; Gillan, C. J.; Carnevali, P.; Liu, B.; Pacansky, J. *Mulliken*, 2.0 ed.; IBM Research Division, Scientific & Technical Application Software, Almaden Research Center: San Jose, CA, 1996.

(19) Frisch, M. J.; Frisch, A.; Foresman, J. B. *Gaussian 94 User's Reference*; Gaussian, Inc.: Pittsburgh, PA, 1996.

ogy.[20] The basis set made use of effective core potentials and is designated LANL2DZ in the Gaussian library.[21−24] This basis set is of double-ζ quality but does not include polarization functions. Because of the long Ir−Ir bond length that we obtained with this basis set (see results), and the long bond lengths surrounding the sulfur atom, on the calculations for $[Ir_2(H)(CO)_2(\mu\text{-}CH_2)(\mu\text{-}SO_2)(dhpm)_2]^+$ (dhpm = $H_2PCH_2PH_2$), we completed additional studies using a modified set of valence p orbitals on the iridium atom as specified by Hall and coworkers.[25] We also added a set of polarization functions to the sulfur atom with an exponent obtained from the database of Feller and coworkers.[26] Minima on the potential energy surface were located using standard methodologies available in Gaussian 94.

The Mulliken software was used on our IBM RS/6000 workstation. We used DFT and made use of the effective core potential basis library called ECP_QD95*. This basis set is of double-ζ quality and includes polarization functions on the nontransition metal atoms. The effective core is of type ECP_CEP-DZ.[27−29] The B3LYP results within Mulliken use the local correlation functional of Perdew and Wang[30] instead of the Vosko et al.[31] which is used in Gaussian 94.[19]

Within both Gaussian 94 and Mulliken, full-geometry optimizations were completed on each of the cations for which we report data. No theoretical vibrational frequencies were computed for any of these species. The bis(diphenylphosphino)methane (dppm) and bis(dimethylphosphino)methane (dmpm) ligands were modeled by replacing the organic substituents on the phosphorus atom with hydrogen atoms to form the bis(dihydrogenphosphino)methane (dhpm) ligand. In all our work we began with the $Ir_2(dhpm)_2$ portion of each molecule in a boatlike configuration, and it retained that configuration throughout the geometry optimization procedure.

In the discussion of the theoretical results (vide infra) we refer to energy differences between different isomers. These are simply differences in internal energy at 0 K. We have not computed vibrational frequencies, so we cannot include any zero-point energy. However, because we are comparing only differences in isomeric energies, the differences in zero-point energy will be miniscule. Furthermore, we will simply compare our differences in internal energy to experimental enthalpy changes.

Results and Characterization of Compounds

Earlier work in this research group and by Eisenberg and co-workers had shown that protonation of the complexes $[Ir_2(CO)_3(dppm)_2]$ (**1**), $[Rh_2(CO)_3(dppm)_2]$, and their heterobinuclear analogue, $[RhIr(CO)_3(dppm)_2]$, yielded the respective hydrido-bridged complexes, $[Ir_2(CO)_2(\mu\text{-}H)(\mu\text{-}CO)(dppm)_2][BF_4]$,[11] $[Rh_2(CO)_2(\mu\text{-}H)(\mu\text{-}CO)(dppm)_2][BF_4]$,[32] and $[RhIr(CO)_3(\mu\text{-}H)(dppm)_2][BF_4]$,[33] by apparent electrophilic attack at the metal−metal bond. An obvious extension of these protonations was to substitute H^+ by CH_3^+ [in the form of methyl triflate (MeOTf), for example] in attempts to obtain methyl-bridged analogues. This expectation was not realized for the Rh-containing complexes, for which an acyl-bridged species was obtained for dirhodium[34] and a product containing a methyl group terminally bound to Ir was obtained for RhIr.[35] The reaction with the diiridium precursor also does not proceed strictly according to expectation, although, as will be explained, a methyl-bridged species is no doubt involved. Instead of the targeted methyl-bridged product, the methylene-bridged hydrido species $[Ir_2(H)(CO)_3(\mu\text{-}CH_2)(dppm)_2][CF_3SO_3]$ (**2**) results from C−H bond cleavage of the methyl group, as shown in Scheme 1.[36] This result parallels an earlier study in which methyl triflate addition to $[Cp^*Ir(\mu\text{-}CO)]_2$ yielded the methylene-bridged hydride $[Cp_2^*Ir_2(CO)_2(\mu\text{-}CH_2)(\mu\text{-}H)][CF_3SO_3]$.[37]

Scheme 1

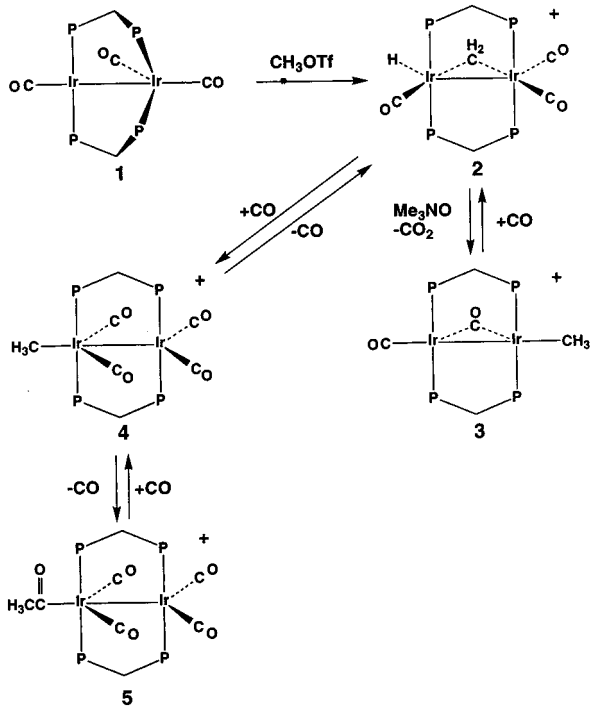

Compound **2** was characterized by extensive spectroscopic investigations. ^1H NMR experiments with selective and broad-band ^{31}P-decoupling, carried out at −40 °C, clearly differentiate the methylene group bridging the metals (δ 4.60) from the two dppm methylene resonances (see Table 1). The Ir_2-bridging methylene appears as an apparent quintet in the ^{31}P-coupled ^1H NMR spectrum and simplifies to a singlet upon broad-band decoupling and to a triplet upon selective decoupling of each ^{31}P resonance in turn, whereas the two ^1H resonances for the dppm methylenes simplify to the expected AB quartet upon broad-band ^{31}P-decoupling. The hydride resonance, which appears as a triplet in the ^1H NMR spectrum at −40 °C, collapses into a singlet upon selectively decoupling the lower field ^{31}P resonance but remains unchanged on decoupling the higher field ^{31}P resonance, showing that it is terminally bound to one of the metals, and is therefore coupling to only the pair of ^{31}P nuclei on this metal.

The $^{13}C\{^1H\}$ NMR spectrum of **2** shows triplets at δ 177.4, 177.0, and 162.0, corresponding to three terminally bound carbonyl groups; and selective ^{31}P-decoupling experiments

(20) Becke, A. D. *J. Chem. Phys.* **1993**, *93*, 5648−5652.
(21) Dunning, T. H., Jr.; Hay, P. J. In *Modern Theoretical Chemistry*; Schaefer, H. F., III, Ed.; Plenum: New York, 1976; pp 1−28.
(22) Hay, P. J.; Wadt, W. R. *J. Chem. Phys.* **1985**, *82*, 270.
(23) Wadt, W. R.; Hay, P. J. *J. Chem. Phys.* **1985**, *82*, 284.
(24) Hay, P. J.; Wadt, W. R. *J. Chem. Phys.* **1985**, *82*, 299.
(25) Couty, M.; Hall, M. B. *J. Comput. Chem.* **1996**, *17*, 1359−1370.
(26) Feller, D.; Schuchardt, K.; Jones, D. *Extensible Computational Chemistry Environment Basis Set Database*, 1.0 ed.; Feller, D., Schuchardt, K., Jones, D., Eds.; Molecular Sciences Computing Facility, Environmental and Molecular Sciences Laboratory, 1998.
(27) Stevens, W.; Basch, H.; Krauss, M. *J. Chem. Phys.* **1984**, *81*, 6026.
(28) Stevens, W.; Jasien, P. G.; Krauss, M.; Basch, H. *Can. J. Chem.* **1992**, *70*, 612.
(29) Cundari, T. R.; Stevens, W. J. *J. Chem. Phys.* **1993**, *98*, 5555.
(30) Perdew, J. P.; Wang, Y. *Phys. Rev. B.* **1992**, *45*, 1324.
(31) Vosko, S. H.; Wilk, L.; Nusair, M. *Can. J. Phys.* **1980**, *58*, 1200.
(32) (a) Kubiak, C. P.; Woodcock, C.; Eisenberg, R. *Inorg. Chem.* **1982**, *21*, 2119. (b) Kubiak, C. P.; Eisenberg, R. *J. Am. Chem. Soc.* **1980**, *102*, 3637.
(33) McDonald, R.; Cowie, M. *Inorg. Chem.* **1990**, *29*, 1564.
(34) Shafiq, F.; Kramarz, K. W.; Eisenberg, R. *Inorg. Chim. Acta* **1993**, *213*, 111.
(35) Antwi-Nsiah, F. H.; Oke, O.; Cowie, M. *Organometallics* **1996**, *15*, 1042.
(36) A preliminary report of this has appeared: Antwi-Nsiah, F.; Cowie, M. *Organometallics* **1992**, *11*, 3157.
(37) Heinekey, D. M.; Michel, S. T.; Schulte, G. K. *Organometallics* **1989**, *8*, 1241.

establish that the high- and low-field carbonyls are bound to one iridium center whereas the third is bound to the other iridium, to which the hydride is also bound. The $^{13}C\{^1H\}$ resonance for the bridging methylene group, obtained on a sample prepared using ^{13}C-methyl triflate, appears as a broad singlet at δ 49.9; the carbon−hydrogen coupling constant ($^1J_{C-H}$ = 140.6 Hz) was obtained from the ^1H NMR spectrum of the ^{13}C-labeled sample.

Although the high-field ^1H resonance could result from either a hydride ligand or an agostic methyl interaction, it can be unambiguously ascribed to a hydride ligand because no $^{13}C-^1H$ coupling is observed. In addition, agostic methyl groups are highly fluxional; for mononuclear complexes we know of no case in which such groups are static on the NMR time scale, even at low temperature,[38] whereas for polynuclear species we know of only two examples in which a static structure (at between −80° and −90 °C) was observed in solution for a bridging agostic methyl group.[39] The observation of separate hydride and methylene signals at the relatively high temperature of −40 °C is more consistent with the formulation shown for **2** than for a bridged agostic methyl interaction.

At temperatures greater than −40 °C the ^1H NMR resonances for the methylene and the hydride ligands of **2** broaden, suggesting an exchange between the two, which has been confirmed by a ^1H NMR, spin−saturation−transfer experiment. Presumably the exchange between the hydride and the methylene hydrogens occurs through an intermediate methyl complex, not unlike the targeted methyl-bridged species. The rates of exchange between the bridging methylene protons and the hydride ligand were determined at various temperatures between −29.7 °C and −56.4 °C, by selective inversion recovery ^1H experiments, and the activation parameters for this exchange process ($\Delta H^{\ddagger} = 10.3 \pm 0.4$ kcal/mol and $\Delta S^{\ddagger} = -11.2 \pm 1.5$ cal/mol K) have been obtained.[40] Compound **2** is therefore the result of an unusually facile and reversible C−H activation of the methyl group.

Compound **2** bears an interesting relationship to two previously reported *dicarbonyl* methyl compounds. In $[Rh_2(CH_3)(CO)(\mu\text{-}CO)(dppm)_2][CF_3SO_3]$[34] the methyl group is *terminally* bound to one rhodium center, whereas in $[Ir_2(CO)_2(\mu\text{-}CH_3)(dmpm)_2][CF_3SO_3]$[41] (dmpm = $Me_2PCH_2PMe_2$) the methyl group *bridges* the metals in a symmetrical fashion. The existence of these dicarbonyl, methyl complexes suggested that CO removal from **2** may *reverse* the C−H bond cleavage step, regenerating a related methyl product. If this were the case, the further question arose as to the subsequent binding mode of the methyl group. The answer to the first suggestion is affirmative; one carbonyl is readily removed from **2** by reaction with Me_3NO, generating the dicarbonyl methyl complex $[Ir_2(CH_3)(CO)_2(dppm)_2][CF_3SO_3]$ (**3**). This species is highly fluxional, so at ambient temperature all spectral parameters suggest a symmetrical species having a bridging methyl group. The $^{31}P\{^1H\}$ NMR spectrum at this temperature shows a singlet at δ 22.1, the ^1H NMR spectrum displays the methyl signal as a quintet at δ 0.58, with equal coupling to all four ^{31}P nuclei, and the $^{13}C\{^1H\}$ NMR spectrum shows one singlet carbonyl resonance at δ 171.4 and a sharp quintet at δ 17.5 ($^2J_{P-C}$ = 4.5 Hz) for the methyl group. However, at low temperatures the spectral parameters are more in keeping with an unsymmetrical species having a terminally bound methyl group. Thus at −80 °C the $^{31}P\{^1H\}$ NMR spectrum shows two resonances for two chemically distinct phosphorus environments (by virtue of the chemically inequivalent metal centers), and the $^{13}C\{^1H\}$ NMR spectrum displays two carbonyl resonances at δ 182.5 and 162.1. In the solid-state ^{13}C NMR spectrum the carbonyl resonances (δ 187.8 and 167.0) are close to those observed in solution at −80 °C, whereas the IR spectrum (Nujol mull) shows carbonyl bands at 1974 and 1832 cm^{-1}, suggesting one terminal and one bridging carbonyl group. Compound **3** is therefore formulated as $[Ir_2(CH_3)(CO)(\mu\text{-}CO)(dppm)_2][CF_3SO_3]$ in the solid state, having a structure much like that of Eisenberg's Rh_2 analogue.[34]

Upon dissolving compound **3**, the strong IR band at 1832 cm^{-1} disappears and is replaced by a *very* weak band at ca. 1886 cm^{-1}, and the stretch caused by the terminal carbonyl moves from 1974 to 1964 cm^{-1}. It would appear that in solution, the dominant species is *not* the same as that found in the solid state, and instead has the structure shown below for **3a**. The

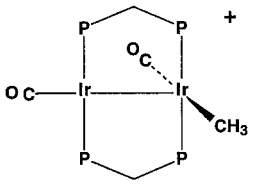

3a

two terminal carbonyls in this compound absorb at approximately the same frequency, giving rise to the broad band at 1964 cm^{-1}. Although this structure type has not, to our knowledge, been observed in dppm-bridged complexes of Rh or Ir, related structures have been observed or proposed for closely related PNP-bridged complexes of rhodium (PNP = $(RO)_2PN(Et)P(OR)_2$)[42] and dppm complexes of platinum and palladium.[43] In addition, as will be addressed later, DFT calculations have shown that structure **3a** is the ground-state structure for the isolated cation. In any case, in all subsequent schemes, compound **3** will be shown having the structure established in the solid state (vide infra).

The fluxionality of **3a**, which gives rise to time-averaged equivalence of both metals, results from transfer of the methyl group from one metal to the other (presumably via a methyl-bridged intermediate) accompanied by slight movement of the carbonyls from opposite the Ir−Ir bond to opposite the methyl group, and vice versa. A full merry-go-round motion of these ligands around the Ir_2P_4 core is ruled out because this would give rise to a time-averaged symmetry on either side of the Ir_2P_4 plane, leading to only one resonance for the dppm methylene hydrogens; at ambient temperature two resonances are observed indicating different environments on either side of the Ir_2P_4 plane.

Confirmation of the proposed structure for **3** *in the solid state* comes from the X-ray structure determination, as shown in Figure 2, with selected distances and angles given in Table 3.

(38) Green, M. L. H.; Hughes, A. K.; Popham, N. A.; Stephens, A. H. H.; Wong, L.-L. *J. Chem. Soc., Dalton Trans.* **1992**, 307.

(39) (a) Park, J. W.; Mackenzie, P. B.; Schaefer, W. P.; Grubbs, R. H. *J. Am. Chem. Soc.* **1986**, *108*, 6402. (b) Ozawa, F.; Park, J. W.; Mackenzie, P. B.; Schaefer, W. P.; Henling, L. M.; Grubbs, R. H. *J. Am. Chem. Soc.* **1989**, *111*, 1319.

(40) Data analysis was carried out according to the method of McClung and co-workers: Muhandiram, D. R.; McClung, R. E. D. *J. Magn. Reson.* **1987**, *71*, 187.

(41) Reinking, M. K.; Fanwick, P. E.; Kubiak, C. P. *Angew. Chem., Int. Ed. Engl.* **1989**, *28*, 1377.

(42) (a) Haines, R. J.; Meintjies, E.; Laing, M. *Inorg. Chim. Acta* **1979**, *36*, L403. (b) Haines, R. J.; Laing, M.; Meintjies, E.; Sommerville, P. *J. Organomet. Chem.* **1981**, *215*, C17.

(43) (a) Brown, M. P.; Cooper, S. J.; Frew, A. A.; Manojlovic-Muir, L.; Muir, K. W.; Puddephatt, R. J.; Seddon, K. R.; Thomson, M. A. *Inorg. Chem.* **1981**, *20*, 1500. (b) Hill R. H.; Puddephatt, R. J. *J. Am. Chem. Soc.* **1983**, *105*, 5797. (c) Xu, C.; Anderson, G. K. *Organometallics* **1996**, *15*, 1760.

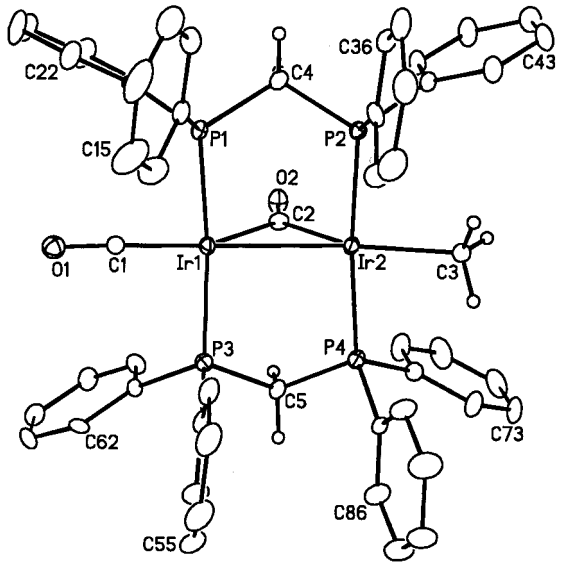

Figure 2. A perspective view of the $[Ir_2(CH_3)(CO)(\mu\text{-}CO)(dppm)_2]^+$ cation of **3**. Thermal ellipsoids are drawn at the 20% level except for methylene and methyl hydrogens which are shown artificially small. Phenyl groups are numbered starting at the ipso carbon, and hydrogens on these groups are omitted.

Table 3. Selected Interatomic Distances and Angles for Compound **3**; X-Ray Data

(a) Distances (Å)

atom 1	atom 2	distance	atom 1	atom 2	distance
Ir(1)	Ir(2)	2.7775(5)	Ir(2)	C(2)	2.089(9)
Ir(1)	P(1)	2.307(2)	Ir(2)	C(3)	2.16(2)
Ir(1)	P(3))	2.308(2)	P(1)	C(4)	1.816(8)
Ir(1)	C(1)	1.77(2)	P(2)	C(4)	1.828(8)
Ir(1)	C(2)	2.110(8)	P(3)	C(5)	1.837(8)
Ir(1)	C(3′)[a]	2.15(2)	P(4)	C(5)	1.825(8)
Ir(2)	P(2)	2.315(2)	O(1)	C(1)	1.19(2)
Ir(2)	P(4)	2.313(2)	O(1′)	C(1′)	1.15(2)
Ir(2)	C(1′)	1.76(2)	O(2)	C(2)	1.095(9)

(b) Angles (deg)

atom 1	atom 2	atom 3	angle	atom 1	atom 2	atom 3	angle
Ir(2)	Ir(1)	C(1)	176.4(6)	P(2)	Ir(2)	P(4)	173.46(8)
Ir(2)	Ir(1)	C(2)	48.3(2)	C(1′)	Ir(2)	C(2)	134.5(7)
Ir(2)	Ir(1)	C(3′)	166.0(5)	C(2)	Ir(2)	C(3)	148.5(6)
P(1)	Ir(1)	P(3)	170.96(8)	Ir(1)	C(1)	O(1)	177.6(16)
C(1)	Ir(1)	C(2)	128.2(7)	Ir(2)	C(1′)	O(1′)	175.8(20)
C(2)	Ir(1)	C(3′)	145.7(6)	Ir(1)	C(2)	Ir(2)	82.8(3)
Ir(1)	Ir(2)	C(1′)	176.6(6)	Ir(1)	C(2)	O(2)	137.9(8)
Ir(1)	Ir(2)	C(2)	48.9(2)	Ir(2)	C(2)	O(2)	138.8(7)
Ir(1)	Ir(2)	C(3)	162.4(5)				

[a] Primed atoms are those of the carbonyl [C(1′)O(1′)] and methyl [C(3′)] groups and are 50:50 disordered with C(1)O(1) and C(3). See the experimental section.

Compound **3** has an unsymmetrical A-frame structure in which one carbonyl group is bridging, but the other carbonyl and the methyl group occupy a terminal position on each metal. These terminal ligands are not opposite the bridging carbonyl, but are in a "flattened A-frame" arrangement being almost trans to the Ir−Ir bond [C(1)−Ir(1)-Ir(2) = 176.4(6)°, Ir(1)−Ir(2)-C(3) = 162.4(5)°]. This arrangement results in somewhat different angles between the bridging carbonyl and the different terminal groups [C(1)−Ir(1)-C(2) = 128.2(7)° and C(2)−Ir(2)-C(3) = 148.5(6)°]. The Ir−Ir separation of 2.7775(5) Å is consistent with a single bond and is shorter than the Rh−Rh separation of 2.811(2) Å in the dirhodium analogue[34]; otherwise the two structures are closely comparable. Although the disorder in the equatorial ligand positions (see Experimental Section) was resolved satisfactorily, the almost superposition of the terminal methyl and carbonyl groups does result in an uncertainty in their exact positions precluding an in-depth discussion of the structural parameters.

The conversion of a hydrido methylene species (**2**) into a methyl complex (**3**) upon removal of a carbonyl group, and the reverse process, C−H bond activation of a methyl group upon addition of a carbonyl ligand, is a fascinating transformation. Usually C−H bond activation in low-valent, late transition-metal complexes is induced by ligand loss to generate the required coordinative unsaturation.[44] We know of one other example of ligand addition resulting in C−H bond activation, in which phosphine addition to a diruthenium complex resulted in cleavage of an agostic C−H bond.[45] It was therefore of interest to determine the scope of the present C−H bond cleavage by reacting compound **3** with several ligands having a range of electronic properties. Although the reactions of **3** with alkynes, allenes, and olefins were also investigated as part of this study, the diversity observed in this series of reactions requires separate reports.[46]

Reaction of **3** with 1 equiv of carbon monoxide regenerates the tricarbonyl complex **2**, accompanied by C−H bond cleavage of the methyl group and formation of the bridging methylene and terminal hydrido groups. This is, of course, essentially the reverse of the conversion of **2** to **3** upon reaction with Me_3NO. Under excess CO compound **2** transforms into a mixture of two tetracarbonyl species, the methyl complex $[Ir_2(CH_3)(CO)_4(dppm)_2][CF_3SO_3]$ (**4**) and the related acyl product $[Ir_2(C(O)CH_3)(CO)_4(dppm)_2][CF_3SO_3]$ (**5**), in varying ratios depending on the CO pressure (see Scheme 1). In compound **4** the methyl resonance appears at δ 0.38 as a triplet in the ^1H NMR spectrum, displaying coupling to the two adjacent phosphorus nuclei, whereas in **5** the ^1H resonance for the methyl group appears as a singlet at δ 0.63. The $^{13}C\{^1H\}$ spectra for both compounds are comparable apart from the low-field resonance for the acyl carbonyl at δ 225.1; this group also displays a characteristic IR stretch at 1622 cm^{-1}. It is an interesting dichotomy that conversion of the methylene and hydrido moieties of **2** into a methyl group occurs *both on addition and removal of CO* (yielding **4** and **3**, respectively). The migratory insertion, transforming **4** to **5**, is readily reversible, so that in the absence of excess CO the mixture of **5** quickly regenerates **4**, and under vacuum **4** transforms quantitatively to **2**.

Reaction of **3** with various phosphines and triphenyl phosphite also results in methyl C−H bond cleavage, yielding the methylene-bridged, hydride products $[Ir_2(H)(CO)_2(PR_3)(\mu\text{-}CH_2)(dppm)_2][CF_3SO_3]$ [PR_3 = PMe_3 (**6**), PMe_2Ph (**7**), PPh_3 (**8**), and $P(OPh)_3$ (**9**)] as shown in Scheme 2. Compounds **6**−**8** all have very similar spectral parameters, apart from the $^{31}P\{^1H\}$ resonances for the monodentate phosphine groups, and also spectrally resemble compound **2** in which a PR_3 group is replaced by CO; therefore all are assumed to have similar structures. This has been confirmed by the X-ray structure determination of **6** (vide infra). However, unlike the tricarbonyl (**2**), the phosphine adducts do not undergo exchange of the hydride and methylene hydrogens at ambient temperature.

(44) (a) Collman, J. P.; Hegedus, L. S.; Norton, J. R.; Finke, R. G. *Principles and Applications of Organotransition Metal Chemistry*; University Science Books: Mill Valley, CA, 1987; pp 298−304, and references therein. (b) Arndtsen, B. A.; Bergman, R. G.; Mobley, T. A.; Peterson, T. H. *Acc. Chem. Res.* **1995**, *28*, 154. (c) All publications in *J. Organomet. Chem* **1995**, *504*, 1−155.

(45) Kuhlman, R.; Folting, K.; Caulton, K. G. *Organometallics* **1995**, *14*, 3188.

(46) (a) A preliminary report of some of this chemistry has appeared: Torkelson, J. R.; McDonald, R.; Cowie, M. *J. Am. Chem. Soc.* **1998**, *120*, 4047. (b) Torkelson, J. R.; McDonald, R.; Cowie, M. Manuscript in preparation.

Scheme 2

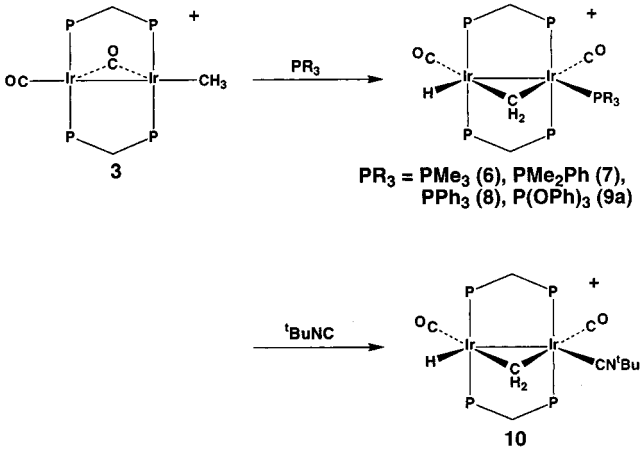

The reaction of **3** with $P(OPh)_3$ actually yields two isomers (**9a** and **9b**). Isomer **9a** has spectral parameters closely resembling those of compounds **6**−**8** so it is assumed to have an analogous structure, whereas the structure of **9b** could not be established conclusively by NMR spectroscopy. The two structures shown below (as **F** and **G**) for isomer **9b** are suggested on the basis of the two carbonyl resonances, one of which is in the region of those in **9a**, suggesting that it also is opposite the μ-CH_2 group, and one of which is clearly in a different environment. We favor structure **F** for **9b**, because both dppm ^{31}P resonances are at similar chemical shifts, suggesting similar environments with one carbonyl on each metal. However we could not carry out a selective ^{31}P-decoupling experiment to conclusively rule out the alternate structure (**G**).

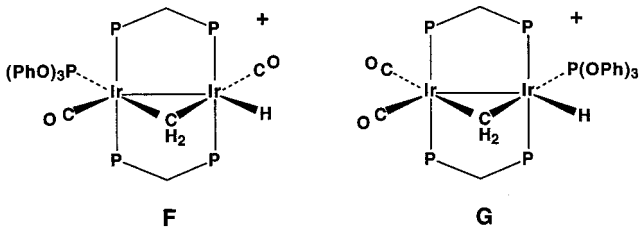

The structure of **6**, as determined by X-ray diffraction is shown in Figure 3. A compilation of important bond lengths and angles is given in Table 4. This structure confirms the methylene-bridged, hydride formulation and also displays the arrangement of carbonyl, hydride, and PMe_3 groups as proposed from the spectral results. The overall geometry is that of an A-frame structure having the carbonyls essentially opposite the bridging methylene group, with the PMe_3 and hydride ligands on the outside of the A-frame, almost bisecting the angles between the μ-CH_2 and terminal carbonyl groups. Both ends of the diphosphine ligands are bent significantly from a trans alignment owing to repulsions involving the PMe_3 group, (P(1)−Ir(1)-P(3) = 163.16(9)° and P(2)−Ir(2)-P(4) = 154.79(8)°). These repulsions may also be responsible for larger Ir−P (dppm) distances at the more crowded Ir(1) center (2.330(2), 2.332(2) Å] than at Ir(2) (2.304(2), 2.305(2) Å], as well as the larger Ir(1)−C(2) distance [2.172(9) Å] compared with Ir(2)−C(2) [2.098(9) Å] involving the methylene group. The angle at the methylene carbon [83.0(3)°] is typical of such a group when bridging a metal−metal bond,[47] as suggested by the short Ir−Ir separation of 2.8308(6) Å.

(47) Herrmann, W. A. *Adv. Organomet. Chem.* **1982**, *20*, 159.

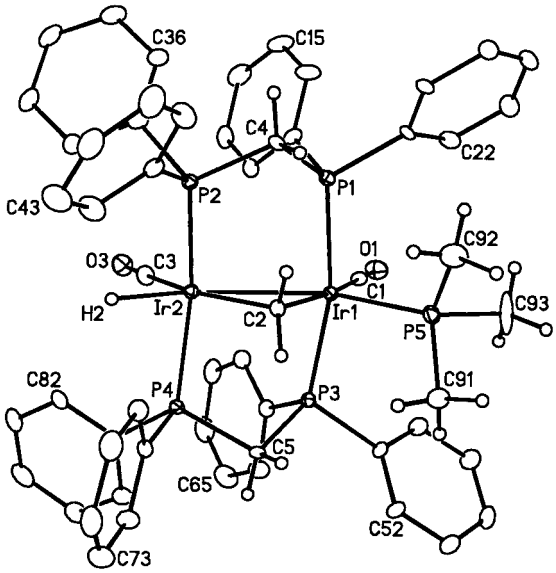

Figure 3. A perspective view of the $[Ir_2H(CO)_2(PMe_3)(\mu\text{-}CH_2)(dppm)_2]^+$ cation of **6**. Thermal parameters and numbering as in Figure 2.

Table 4. Selected Interatomic Distances and Angles for Compound **6**; X-Ray Data

(a) Distances (Å)

atom 1	atom 2	distance	atom 1	atom 2	distance
Ir(1)	Ir(2)	2.8308(6)	Ir(2)	C(3)	1.909(9)
Ir(1)	P(1)	2.332(2)	Ir(2)	H(2)	1.71
Ir(1)	P(3)	2.330(2)	P(1)	C(4)	1.819(9)
Ir(1)	P(5)	2.359(3)	P(2)	C(4)	1.830(9)
Ir(1)	C(1)	1.887(9)	P(3)	C(5)	1.818(9)
Ir(1)	C(2)	2.172(9)	P(4)	C(5)	1.850(9)
Ir(2)	P(2)	2.304(2)	O(1)	C(1)	1.141(11)
Ir(2)	P(4)	2.305(2)	O(3)	C(3)	1.117(12)
Ir(2)	C(2)	2.098(9)			

(b) Angles (deg)

atom 1	atom 2	atom 3	angle	atom 1	atom 2	atom 3	angle
Ir(2)	Ir(1)	P(5)	131.72(7)	C(2)	Ir(2)	C(3)	157.9(4)
Ir(2)	Ir(1)	C(1)	123.3(3)	Ir(1)	P(5)	C(91)	116.7(4)
Ir(2)	Ir(1)	C(2)	47.4(2)	Ir(1)	P(5)	C(92)	116.9(5)
P(1)	Ir(1)	P(3)	163.16(9)	Ir(1)	P(5)	C(93)	115.5(4)
P(5)	Ir(1)	C(1)	104.9(3)	C(91)	P(5)	C(92)	99.5(6)
P(5)	Ir(1)	C(2)	84.4(2)	C(91)	P(5)	C(93)	102.6(7)
C(1)	Ir(1)	C(2)	170.7(4)	C(92)	P(5)	C(93)	103.2(8)
Ir(1)	Ir(2)	C(3)	108.3(3)	Ir(1)	C(1)	O(1)	178.5(9)
Ir(1)	Ir(2)	C(2)	49.6(2)	Ir(1)	C(2)	Ir(2)	83.0(3)
P(2)	Ir(2)	P(4)	154.79(8)	Ir(2)	C(3)	O(3)	177.4(9)

The reaction of **3** with ^{t}BuNC also occurs readily, producing the C−H-activated product $[Ir_2(H)(CO)_2(CN^tBu)(\mu\text{-}CH_2)(dppm)_2][CF_3SO_3]$ (**10**) analogous to the phosphine adducts (**6**−**9a**). As with the phosphine adducts, no exchange between the hydride and methylene protons is observed at ambient temperature. All spectroscopic parameters support the structure shown, and in particular, the characteristic C≡N stretch in the IR spectrum for the ^{t}BuNC appears at 2163 cm^{-1}, consistent with this group being terminally bound.[48] The increase in frequency of the C≡N stretch compared with that in free ^{t}BuNC (2125 cm^{-1}) is consistent with this group functioning primarily as a σ donor. As for the CO (**2**) and PR_3 (**6**−**9**) adducts, no Ir−H stretch could be detected in the IR spectrum of compound **10**.

(48) (a) Treichel, P. M. *Adv. Organomet. Chem.* **1973**, *11*, 21. (b) Lukehart, C. *Fundamental Transition Metal Organometallic Chemistry*; Brooks/Cole Publishing Company: Belmont, CA, 1985; p 77.

The reaction of compound **3** with SO_2 appears to be somewhat analogous to the reactions with CO, phosphines, and ^{t}BuNC, producing a methylene-bridged, hydrido complex $[Ir_2(H)(CO)_2(\mu\text{-}CH_2)(\mu\text{-}SO_2)(dppm)_2][CF_3SO_3]$ (**11**). Like the CO adduct (**2**), compound **11** is fluxional, undergoing facile exchange of the hydride ligand and the methylene hydrogens. The unusually facile exchange process in **11** (vide infra) caused some initial uncertainty about its formulation, because it was necessary to rule out a species, $[Ir_2(CO)_2(\mu\text{-}\eta^1,\eta^2\text{-}CH_3)(\mu\text{-}SO_2)(dppm)_2][CF_3SO_3]$, containing an asymmetrically bound methyl group of the type shown in structure **E**. In this case hydrogen exchange would occur by rotation about the Ir−CH_3 bond, interchanging the agostic interaction between the three C−H bonds. At ambient temperature the $^{31}P\{^1H\}$ NMR spectrum appears as a singlet at δ −1.0, consistent with the chemical equivalence of all four phosphorus nuclei. In the ^1H NMR spectrum the three hydrogens of the methyl group appear as a broad singlet at δ −2.15, with coupling of 98 Hz observed to carbon when $^{13}CH_3^+$ is used. At 50 °C the "CH_3 signal" appears as a well-resolved quintet, coupling equivalently to all four phosphorus nuclei. The high-field shift of this resonance and the small average C−H coupling constant are consistent with a fluxional process involving either the methylene-hydride or the agostic methyl formulations, although the average value of $^1J_{C-H}$ is slightly lower than has previously been suggested for asymmetrically bridged methyl groups.[49] At ambient temperature the ^{13}C NMR spectra add additional support for the symmetric time-averaged structure with only one signal (at δ 170.8) for both carbonyls and a sharp quartet at δ 36.8 for the methyl carbon, showing equivalent coupling to the three hydrogens.

Lowering the temperature causes the methyl resonance in the ^1H NMR spectrum to broaden until at −60 °C the signal has fully collapsed into the baseline. At −110 °C a very broad signal at ca. δ 4.2 (2H) and an equally broad signal at ca. δ −14.6 (1H) start to appear, but are only barely discernible above the baseline. Support for the exchange process was shown by irradiating the low-field signal at −110 °C and observing that the high-field signal disappeared (although the barely discernible signal at this temperature makes such a conclusion equivocal). The activation parameters for this exchange process ($\Delta H^{\ddagger} = 6.1 \pm 0.1$ kcal/mol and $\Delta S^{\ddagger} = -6.2 \pm 0.5$ cal/mol K) were obtained from a line-shape analysis on variable-temperature ^1H NMR spectra.[50] At the outset, these activation parameters appeared to us to be too small to correspond to a C−H bond-cleavage process, being about half the value obtained in the tricarbonyl compound, **2**, and much less than values near 20 kcal/mol previously observed in binuclear systems.[51] On the other hand, these values are in line with the activation energy ($\Delta G^{\ddagger} = 9.8$ kcal/mol) for exchange of the methyl hydrogens in a bridging agostic methyl interaction, by rotation about the metal−carbon bond.[39]

Attempts to prepare compound **11** with d^3-methyl triflate resulted in partial hydrogen incorporation (presumably from solvent) such that the desired product was contaminated with small, but significant amounts of the CHD_2, CH_2D, and CH_3 isotopomers. This inadvertent result presented us with the opportunity to investigate the effects of isotopic perturbation of resonance (IPR) in compound **11**. Although first described by Saunders et al.[52] in studies of carbocations, this effect was later used (first by Calvert and Shapley[53] and subsequently by others[10a,54]) to help establish the presence of agostic interactions involving methyl groups. Owing to zero-point energy differences an agostic interaction of a C−H bond is favored over that of a C−D bond. As a result, the ^1H chemical shift of an agostic CHD_2 group appears at a higher field than that of a CH_2D group, which is in turn at a higher field than that of a CH_3 group. Furthermore, the chemical shifts of the CHD_2 and CH_2D groups are also temperature dependent, shifting upfield at lower temperatures; this effect is greater for CHD_2 than for CH_2D. The ^1H NMR spectrum in the methyl region for compound **11**, which was prepared from d^3-methyl triflate, is shown in Figure 4, and the temperature variation of the chemical shifts is presented in Table 5. Although these results clearly demonstrate the IPR phenomenon, consistent with hydrogen exchange between the agostic and anagostic hydrogens, they do not by themselves establish the existence of an agostic interaction, because it has been pointed out that this effect will also be observed in a system in which facile exchange occurs between a hydrido ligand and methylene hydrogens.[49] From the IPR data, the chemical shifts for the two different hydrogen environments are calculated[49b,53] at δ 4.13 and −14.47. It is encouraging that these values are in very close agreement with the positions of the very broad resonances that are beginning to appear in the

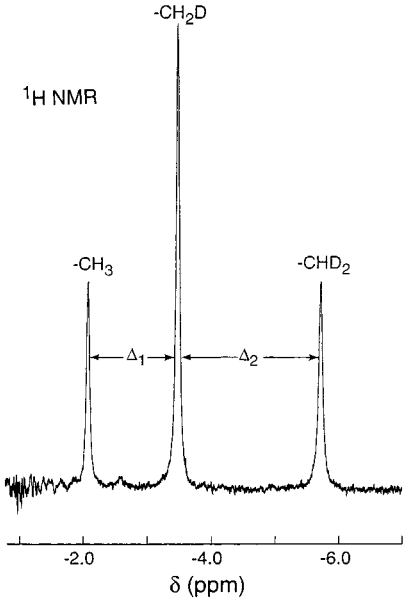

Figure 4. ^1H NMR spectrum in the "methyl" region for the CH_3, CH_2D, and CH_2D isotopomers of compound **11**.

Table 5. Variation of Chemical Shift with Temperature for the Isotopomers of Compound **11**

temp (°C)	$\delta(CH_3)$	$\delta(CH_2D)$	$\delta(CD_2H)$	Δ_1	Δ_2
25	−2.07	−3.48	−5.72	1.41	2.24
10	−2.05	−3.52	−5.90	1.47	2.38
0	−2.05	−3.56	−6.02	1.51	2.46
−20	−2.02	−3.62	−6.40	1.60	2.78

[a] For a definition of Δ_1 and Δ_2 see Figure 4.

(49) (a) Brookhart, M.; Green, M. L. H.; Wong, L.-L. *Prog. Inorg. Chem.* **1988**, *36*, 1. (b) Tolman, C. A.; Faller, J. W. In *Homogeneous Catalysis with Metal Phosphine Complexes;* Pignolet, L. H., Ed.; Plenum Press: New York, 1983; pp 30−34.

(50) (a) The program used was *NMR Exchange* for Windows 95, written by R. E. D. McClung, 1997. (b) McConnell, H. M. *J. Chem. Phys.* **1958**, *28*, 430.

(51) Jacobsen, E. N.; Goldberg, K. I.; Bergman, R. G. *J. Am. Chem. Soc.* **1988**, *110*, 3706.

(52) Saunders: M.; Jaffe, M. H.; Vogel, P. *J. Am. Chem. Soc.* **1971**, *93*, 2558.

(53) Calvert, R. B.; Shapley, J. R. *J. Am. Chem. Soc.* **1978**, *100*, 7726.

(54) See for example: (a) Casey, C. P.; Fagan, P. J.; Miles, W. H. *J. Am. Chem. Soc.* **1982**, *104*, 1134. (b) Green, M. L. H.; Hughes, A. K.; Popham, N. A.; Stephens, A. H. H.; Wong, L.-L. *J. Chem. Soc., Dalton Trans.* **1992**, 3077.

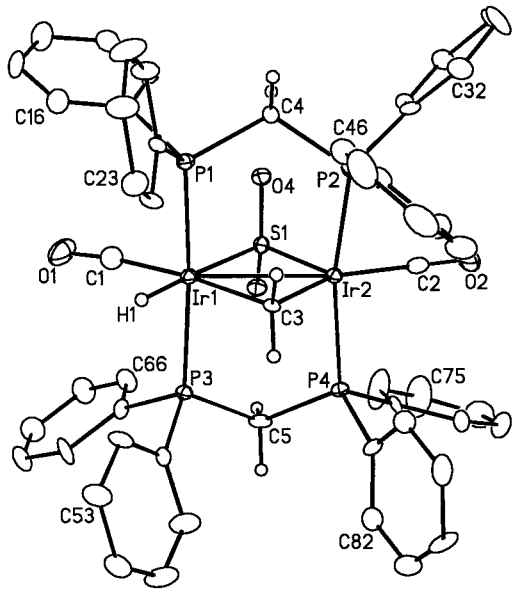

Figure 5. A perspective view of the $[Ir_2H(CO)_2(\mu\text{-}CH_2)(\mu\text{-}SO_2)(dppm)_2]^+$ cation of **11**. Thermal parameters and numbering as in Figure 2. The hydride ligand [H(1)] and the hydrogens on C(3) were not located in the X-ray study, but are placed in idealized positions.

^{1}H NMR spectrum at −110 °C. Furthermore, the chemical shift of the low-field signal is more consistent with a methylene group than a methyl group. This conclusion is supported by the low average value of $^1J_{C-H}$ (98 Hz), which would then result from averaging of the two single-bond coupling constants of $^1J_{C-H} \approx 147$ Hz with a two-bond coupling (between the methylene carbon and the hydride ligand) of $^2J_{C-H} \approx 0$ Hz. The C−H coupling constant proposed for the methylene group is in good agreement with previous determinations.[55]

In hopes of establishing conclusively (at least in the solid state) whether compound **11** contained an agostic methyl group or methylene and hydride groups, the X-ray structure determination of **11** was undertaken. Unfortunately, the conclusions were equivocal here also. Our only successful attempts to obtain suitable crystals were from CH_2Cl_2 solvent, from which the desired crystals were always contaminated by varying amounts of $[Ir_2(CO)_2(\mu\text{-}Cl)(\mu\text{-}SO_2)(dppm)_2][CF_3SO_3]$,[16] which resulted from replacement of the methyl group by a chlorine atom (crystals of compound **11** and this chloro-bridged species are isomorphous). The resulting placement of the fractional occupancy chloro ligand on top of the CH_3 or CH_2 group prevents location of the attached hydrogens; however, the metrical parameters of the complex (vide infra) are consistent with the methylene-hydride formulation suggested by the NMR study.

An ORTEP diagram for compound **11** is shown in Figure 5 with important bond lengths and angles given in Table 6. Compound **11** has the SO_2 group in a bridging arrangement with the carbonyl ligands bound terminally, one on each metal. Although the hydrogen atoms originating on the methyl group of the precursor (**3**) could not be located, C(3) is assumed to be associated with a methylene group which bridges the metals on the face opposite the SO_2 group; the hydride ligand and the methylene hydrogens have been idealized in the positions shown. Excluding the metal−metal bond the geometry around the metals is best described as octahedral at Ir(1) and trigonal bipyramidal at Ir(2), with both diphosphine groups in the expected trans arrangements [P(1)−Ir(1)−P(3) = 170.6(1)° and P(2)−Ir(2)−P(4) = 161.9(1)°]. The SO_2 group bridges in an asymmetric manner with the Ir(1)−S(1) bond length [2.449(3) Å] longer than the Ir(2)−S(1) bond length [2.273(3) Å]; this difference is consistent with the high trans influence of the hydride ligand, which is assumed to be in the vacant coordination site on Ir(1) opposite S(1).

(55) See for example, compound **2** and refs 49a and 54.

Table 6. Selected Interatomic Distances and Angles for Compound **11**; X-Ray Data

(a) Distances (Å)

atom 1	atom 2	distance	atom 1	atom 2	distance
Ir(1)	Ir(2)	2.8534(7)	Ir(2)	C(2)	1.85(2)
Ir(1)	Cl(1)	2.66(2)	Ir(2)	C(3)	2.123(14)
Ir(1)	S(1)	2.449(3)	S(1)	O(3)	1.459(8)
Ir(1)	C(1)	1.88(2)	S(1)	O(4)	1.450(8)
Ir(1)	C(1′)[a]	1.85[b]	O(1)	C(1)	1.16(2)
Ir(1)	C(3)	2.190(12)	O(1′)	C(1′)	1.15[a]
Ir(2)	Cl(1)	2.68(2)	O(2)	C(2)	1.14(2)
Ir(2)	S(1)	2.273(3)	Ir(2)	P(2)	2.337(3)
Ir(1)	P(1)	2.353(3)	Ir(2)	P(4)	2.330(3)
Ir(1)	P(3)	2.364(3)			

(b) Angles (deg)

atom 1	atom 2	atom 3	angle	atom 1	atom 2	atom 3	angle
Ir(2)	Ir(1)	S(1)	50.06(7)	Ir(1)	Ir(2)	C(3)	49.6(3)
Ir(2)	Ir(1)	C(1)	141.6(5)	Cl(1)	Ir(2)	C(2)	141.3(7)
Ir(2)	Ir(1)	C(1′)	170.3(32)	S(1)	Ir(2)	C(2)	105.6(5)
Ir(2)	Ir(1)	C(3)	47.6(4)	S(1)	Ir(2)	C(3)	105.3(3)
Cl(1)	Ir(1)	C(1′)	130.7(32)	P(2)	Ir(2)	P(4)	161.90(11)
S(1)	Ir(1)	C(1)	91.6(5)	C(2)	Ir(2)	C(3)	149.1(6)
S(1)	Ir(1)	C(1′)	120.9(33)	Ir(1)	Cl(1)	Ir(2)	64.6(5)
S(1)	Ir(1)	C(3)	97.6(4)	Ir(1)	S(1)	Ir(2)	74.24(8)
P(1)	Ir(1)	P(3)	170.60(10)	Ir(1)	C(1)	O(1)	172.3(17)
C(1)	Ir(1)	C(3)	170.7(6)	Ir(1)	C(1′)	O(1′)	175.7(77)
Ir(1)	Ir(2)	Cl(1)	57.4(5)	Ir(2)	C(2)	O(2)	177.4(16)
Ir(1)	Ir(2)	S(1)	55.70(8)	Ir(1)	C(3)	Ir(2)	82.8(5)
Ir(1)	Ir(2)	C(2)	161.3(5)				

[a] Primed atoms belong to $[Ir_2(CO)_2(\mu\text{-}Cl)(\mu\text{-}SO_2)(dppm)_2][CF_3SO_3]$ which is superimposed on compound **11** in a 12.5:87.5 disorder. [b] Distance fixed (within 0.01 Å of this value) during refinement.

Although the crystallographic data do not unambiguously differentiate between an asymmetrically bridged methyl group and a methylene-bridged hydride structure, the structural parameters are more supportive of the latter assignment. It is clear that carbonyl group C(1)O(1) is bent back toward the μ-SO_2 group compared with C(2)O(2) [Ir(2)−Ir(1)−C(1) = 141.6(5)°, Ir(1)−Ir(2)−C(2) = 161.3(5)°] giving rise to a larger C(1)−Ir(1)−C(3) angle [170.7(6)°] than the C(2)−Ir(2)−C(3) angle of 149.1(6)°, and suggesting the location of the hydride ligand in the resulting vacant site, as shown in Figure 5. All spectroscopic and crystallographic data together support the methylene-bridged, hydride structure for compound **11**, as do the DFT calculations reported below.

Reaction of compound **11** with CO parallels that of the methylene-bridged tricarbonyl (**2**), yielding the SO_2-bridged, tricarbonyl methyl species, $[Ir_2(CH_3)(CO)_3(\mu\text{-}SO_2)(dppm)_2][CF_3SO_3]$ (**12**), in which the methyl group is now terminally bound to one of the metals. The three carbonyls are also shown to be terminally bound, on the basis of ^{13}C NMR and IR spectroscopy. Although the relative positions of the methyl and μ-SO_2 groups are not known, the geometry shown for **12** in Scheme 3 is based on the assumption that hydride transfer from Ir to the methylene group, yielding a methyl group σ-bound to the adjacent metal, would leave coordinative unsaturation at the first metal, which would be alleviated by CO coordination. In a further parallel of the reaction of **2** with CO, compound **12** reacts further with CO to produce the acyl compound $[Ir_2(CH_3CO)(CO)_3(\mu\text{-}SO_2)(dppm)_2][CF_3SO_3]$ (**13**), as shown by the loss of coupling for the methyl group which now appears as a singlet in the ^{1}H

Scheme 3

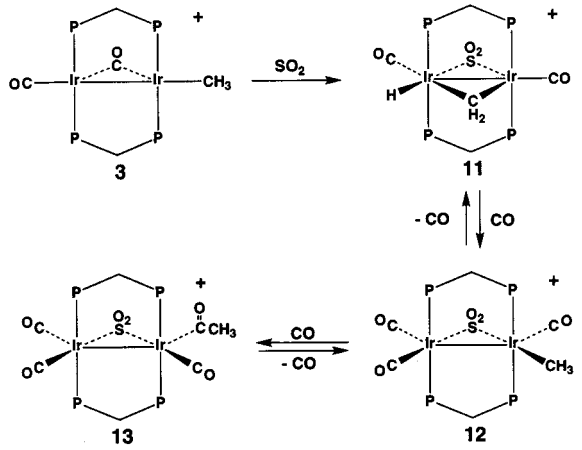

NMR spectrum at δ 1.28, and by the IR spectrum which shows an acyl band at 1646 cm^{-1}. Again the geometry shown for **13** is not known but the structure shown is based on the assumed migration of the methyl group to the adjacent carbonyl on the same metal.

Theoretical Results

We have carried out DFT calculations on two different cationic species related to compounds **3** and **11** and on isomers of each, in efforts to learn more about the bonding involving the methyl groups and about the C−H bond-activation process of methyl groups in the vicinity of adjacent metals. The first compound investigated was $[Ir_2(CH_3)(CO)_2(dhpm)_2]^+$ (**IIIt**); this is the analogue of **3** in which the phenyl substituents on the bridging diphosphine ligands were input as hydrogens to facilitate the calculations (i.e., dhpm = $H_2PCH_2PH_2$). Calculations on the related A-frame, $[Ir_2(CO)_2(\mu\text{-}CH_3)(dhpm)_2]^+$, in which the methyl group now bridges the metals, were also carried out in attempts to establish which (if any) of the above-mentioned structures (terminal or bridging CH_3) was favored for the isolated cation, and how the energies of these isomers compared. In our calculations, the structure having a terminal methyl group is labeled (**IIIt**), whereas the dhpm analogue of Kubiak's methyl-bridged compound[41] is labeled **IIIb**.

Using the X-ray coordinates of **3** as a starting point for the calculations on **IIIt**, we looked for an energy minimum corresponding to the X-ray-derived structure of **3**. Surprisingly, the calculations did not converge to a structure close to that input, but instead the bridging carbonyl migrated away from the bridging site, with concomitant movement of the methyl group, yielding the geometry shown in Figure 6a. In the computed structure **IIIt**, the square plane about Ir(2), defined by P(2), P(4), C(2), and C(3), is not perpendicular to the Ir(1)−Ir(2) vector, but is tilted significantly such that the carbonyl C(2)O(2) is tipped toward Ir(1), with the methyl group tipped away [Ir(1)−Ir(2)−C(2) = 78.6°; Ir(1)−Ir(2)−C(3) = 111.6°]. This tilt may be favored by the retention of a small component of π back-bonding from Ir(1) to C(2)O(2). It is significant that the proposed structure of **3** in solution (**3a**) corresponds to that calculated for the isolated cation, having a geometry rather different from that in the solid state. The transformation from the solid-state structure of **3** to that calculated for **IIIt** involves very little change at Ir(1), because in both structures carbonyl C(1)O(1) is essentially opposite the metal−metal bond. The change primarily involves twisting of the O(2)C(2)−Ir(2)−C(3) unit so that C(2)O(2) moves away from the bridging position.

We next carried out calculations on $[Ir_2(CO)_2(\mu\text{-}CH_3)(dhpm)_2]^+$ (isomer **IIIb**), in which the methyl group in **IIIt** has moved from a terminal position to a bridging site. Mulliken computational studies on two isomers of **IIIb** have been carried out; in the first, the methyl group is unsymmetrically bridged, involving an agostic interaction, as shown earlier in structure **E**, whereas the second isomer has the methyl group bridging symmetrically (structure **D**). Both results are shown in Figure 6b and 6c, respectively. The unsymmetrically bridged isomer is more stable by only 0.8 kcal/mol, and significantly, even the more stable methyl-bridged structure is approximately 6 kcal/mol *less stable* than structure **IIIt**, having the terminal methyl group. Table 7 contains a comparison of the pertinent geometric features of these three isomers [**IIIt**, **IIIb** (**agostic**), and **IIIb** (**symmetric**)]. In general, the parameters for **IIIb** (**symmetric**) agree reasonably well with those of the X-ray determination of the dmpm analogue,[41] and in particular the calculated Ir−Ir bond length is comparable with that in the X-ray structure.

Although conversion of the methyl compound **3** to the respective methylene hydride products requires the addition of small molecules such as CO, PR_3, ^{t}BuNC, and SO_2, it is not clear whether ligand addition induces C−H bond cleavage or whether *prior* C−H bond activation in **3** occurs to yield

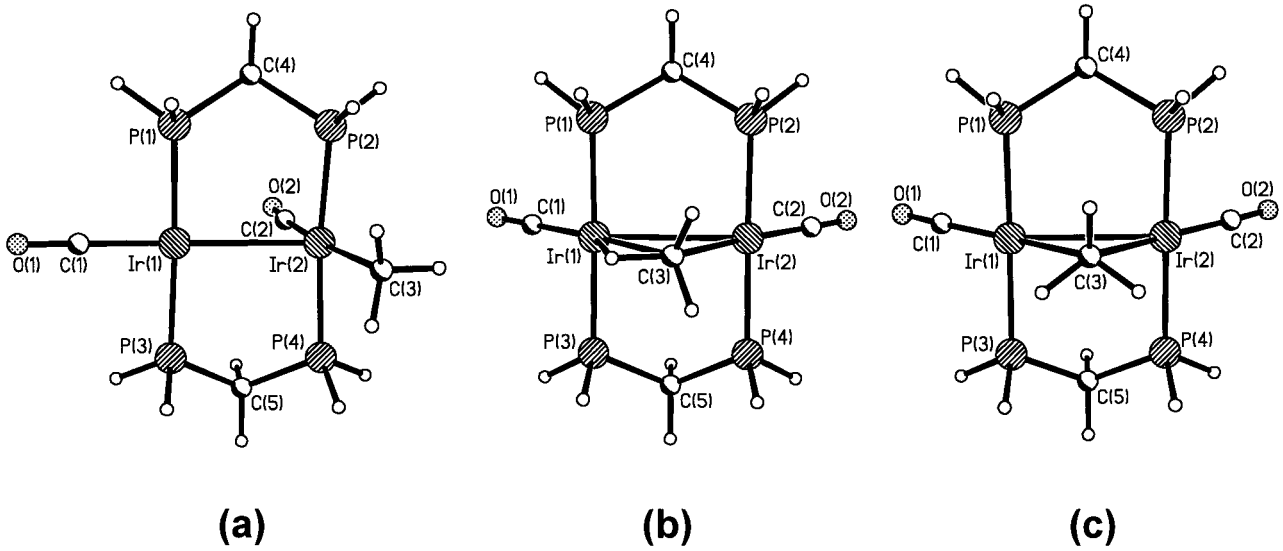

Figure 6. The calculated structures of three isomers of the $[Ir_2(CH_3)(CO)_2(dhpm)_2]^+$ cation: (a) structure **IIIt**; (b) structure **IIIb** (**agostic**); (c) structure **IIIb** (**symmetric**).

Table 7. Geometric Features Calculated for Structures **IIIt**, Both Agostic and Symmetric Methyl-Bridged Structures of **IIIb**, and Structures **IIIh** and **III-TS**

atom 1	atom 2	atom 3	structure **IIIt**	structure **IIIb (agostic)**	structure **IIIb (symmetric)**	structure **IIIh**	structure **III-TS**
				Distances (Å)			
Ir(1)	Ir(2)		2.84	2.99	2.99	2.98	3.07
Ir(1)	C(3)		4.14	2.37	2.34	2.09	2.16
Ir(2)	C(3)		2.14	2.30	2.34	2.19	2.17
Ir	P (av)		2.34	2.34	2.34	2.33	2.33
Ir(1)	C(1)		1.84	1.85	1.86	1.96	1.92
Ir(2)	C(2)		1.93	1.87	1.86	1.91	1.90
Ir(1)	H(1)			2.09	2.92	1.59	1.62
C(3)	H(1)		1.10	1.13	1.09		1.80
				Angles (deg)			
Ir(1)	C(3)	Ir(2)		79.6	79.6	88.3	90.3
Ir(1)	Ir(2)	C(2)	78.6	135.8	138.8	129.6	132.7
Ir(1)	Ir(2)	C(3)	111.6	51.2	50.2	44.4	44.7
Ir(2)	Ir(1)	C(3)		49.2	50.2	47.3	44.9
P	Ir	P	174.5	177.1	177.8	170.8	175.2
C(2)	Ir(2)	C(3)	169.8	173.1	170.6	174.0	177.4
C(1)	Ir(1)	C(3)		173.9	170.6	167.7	175.6
C(1)	Ir(1)	H(1)		145.5		90.4	121.1
C(3)	Ir(1)	H(1)		28.5		101.8	54.5

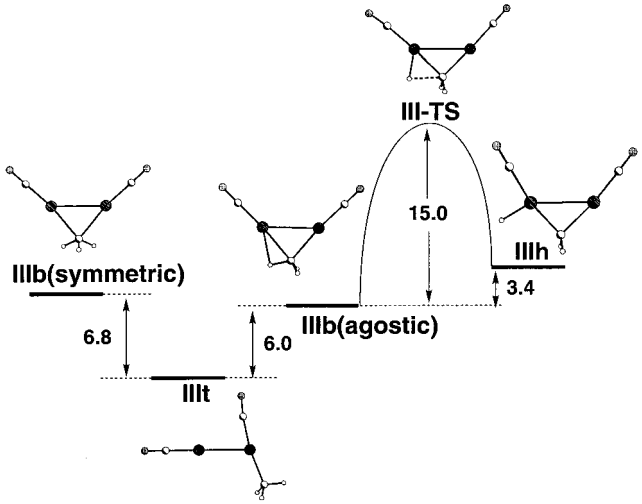

Figure 7. Potential energy diagram for the different isomers of the $[Ir_2(CH_3)(CO)_2(dhpm)_2]^+$ cation **III**. Energies in kcal/mol. Molecular drawings are shown with the dhpm ligands, above and below the plane of the paper, omitted for clarity.

undetectable amounts of a methylene hydride $[Ir_2H(CO)_2(\mu\text{-}CH_2)(dppm)_2]^+$ which subsequently reacts with the added ligands to yield the final products. We have therefore carried out DFT calculations on the dhpm analogue of this methylene hydride cation (called **IIIh**; "h" signifies hydride) and a drawing of the equatorial plane of this species (phosphine ligands omitted) appears in Figure 7 (which shows the relative energies of all isomers of **III**), with calculated bond lengths and angles in Table 7. This structure is only 3.4 kcal/mol less stable than structure **IIIb** (**agostic**). A transition state between **IIIb** (**agostic**) and **IIIh** has been located at an energy of about 15.0 kcal/mol above that of the agostic structure.[56] A drawing of the equatorial plane of this transition-state structure (labeled **III-TS**) is shown in Figure 7, and important structural parameters are given in Table 7. Structure **III-TS** very much resembles **IIIh** except that the hydrido ligand is substantially closer to the methylene group (1.80 vs 2.87 Å) but still retains hydride character, having a normal Ir−H distance of 1.62 Å.

The initial ambiguities about the fate of the methyl group (i.e., CH_3 or μ-CH_2/H) in the SO_2 adduct **11** led us to carry out DFT calculations, using Gaussian 94 software, on this species. Again, the X-ray-derived positions were used as a starting point for the $[Ir_2H(CO)_2(\mu\text{-}CH_2)(\mu\text{-}SO_2)(dhpm)_2]^+$ cation (**XIh**; "h" signifies hydride). It is encouraging that geometry optimization yields a structure that agrees with the methylene hydride formulation deduced from the NMR and X-ray results. The calculated geometry is diagrammed in Figure 8a. The most notable discrepancy between the calculated and X-ray structures is the Ir−Ir distance, which was 0.47 Å too long (3.32 vs 2.85 Å) in the initial calculations. This discrepancy in Ir−Ir bond length is surprising because all other structures calculated in this article have the expected metal−metal separations; and in particular, the structure of **IIIb**, involving the symmetrically bridged methyl group, is close to the crystallographic value for the dmpm analogue. The Couty/Hall modification to the valence p orbitals of the Ir atom in the Gaussian 94 calculations did not provide much change in any of the parameters. However, addition of a polarization orbital to the S atom in the Gaussian 94 calculations resulted in significant improvement to the Ir−S and S−O distances. The effect of the combined change in the Ir p orbital and the polarization orbital on the S atom was to decrease the Ir−Ir distance from 3.32 to 3.21 Å—an improvement, but still a long way from the experimental (X-ray) result of 2.85 Å. Scanning the remainder of the bond lengths in Table 8, we see that Gaussian 94 (with modifications to the Ir p orbital and added polarization function on the S atom) and Mulliken results give overall best agreement with experiment.

Despite the discrepancy between calculations and experiment (Table 8), there is a remarkable correlation in the asymmetry of binding in the SO_2 ligand in all models. The experimental asymmetry in SO_2 binding [(Ir(1)−S(1))−(Ir(2)−S(1))] is 0.18 Å, whereas the four theoretical results give asymmetries of 0.16, 0.15, 0.15, and 0.13 Å. We previously attributed this asymmetry to the trans influence of the hydride ligand. Among the angles in Table 8, there are several involving C(3) which deviate from experiment by as much as 10−15°; most of these can be attributed to the long Ir−Ir distance noted above. One exception

(56) We were unable to locate the transition state between **IIIb (agostic)** and **IIIh** by using automated procedures in the Mulliken software. Therefore, we completed a linear synchronous transit calculation connecting **IIIb (agostic)** with **IIIh**. Then we picked selected points near the top of the energy barrier, and carried out several additional calculations in which we optimized all of the parameters except the Ir−Ir−H angle. We believe that we have located the transition state by this means to within 0.5 kcal/mol. Additional studies are in progress to further examine the nature of the transition state for this system.

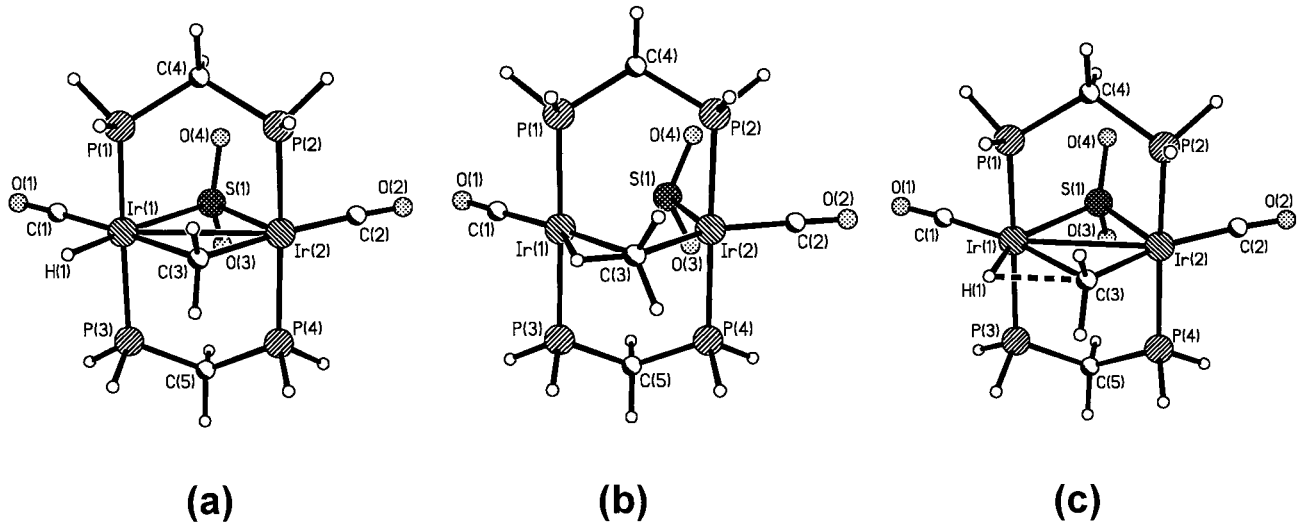

Figure 8. The calculated structures of two isomers of the $[Ir_2(CH_3)(CO)_2(\mu\text{-}SO_2)(dhpm)_2]^+$ cation; (a) $[Ir_2H(CO)_2(\mu\text{-}CH_2)(\mu\text{-}SO_2)(dhpm)_2]^+$ (**XIh**) and (b) $[Ir_2(CO)_2(SO_2)(\mu\text{-}CH_3)(dhpm)_2]^+$ (**XIa**), and (c) the transition state (**XI-TS**) between them.

Table 8. Comparison of Geometries of the Different Calculated Models for Structure **XIh** and that of the X-Ray Structure of Compound **11**

(a) Bond Lengths (Å)

atom 1	atom 2	expt[a]	G94[b] B3LYP	G94 (with mod Ir p orb)	G94 (with mod Ir p orb and S d orb)	Mulliken B3LYP
Ir(1)	Ir(2)	2.85	3.32	3.29	3.21	3.24
Ir(1)	S(1)	2.45	2.64	2.61	2.52	2.54
Ir(1)	P(1)	2.35	2.41	2.40	2.40	2.35
Ir(1)	P(3)	2.36	2.41	2.41	2.40	2.35
Ir(1)	C(1)	1.88	1.94	1.94	1.93	1.95
Ir(1)	C(3)	2.19	2.18	2.18	2.20	2.19
Ir(1)	H(1)	1.70[c]	1.58	1.58	1.60	1.61
Ir(2)	S(1)	2.27	2.48	2.46	2.37	2.41
Ir(2)	P(2)	2.34	2.41	2.41	2.41	2.36
Ir(2)	P(4)	2.33	2.41	2.41	2.41	2.36
Ir(2)	C(2)	1.85	1.93	1.93	1.93	1.94
Ir(2)	C(3)	2.12	2.13	2.13	2.12	2.14
S(1)	O(3)	1.46	1.64	1.64	1.50	1.48
S(1)	O(4)	1.45	1.64	1.64	1.50	1.48
O(1)	C(1)	1.16	1.17	1.17	1.17	1.15
O(2)	C(2)	1.14	1.17	1.17	1.18	1.15

(b) Bond Angles (deg)

atom 1	atom 2	atom 3	expt[a]	G94[b] B3LYP	G94 (with mod Ir p orb)	G94 (with mod Ir p orb and S d orb)	Mulliken B3LYP
Ir(2)	Ir(1)	S(1)	50.1	47.6	56.4	50.9	47.4
Ir(2)	Ir(1)	C(1)	143.5	143.4	143.2	142.1	142.5
Ir(2)	Ir(1)	C(3)	47.6	39.1	39.5	41.1	40.9
Ir(2)	Ir(1)	H(1)	125[c]	123.6	123.8	124.6	125.6
S(1)	Ir(1)	C(1)	93.5	95.8	86.9	95.1	95.2
S(1)	Ir(1)	H(1)	175[c]	171.2	177.7	171.6	173.0
P(1)	Ir(1)	P(3)	170.6	169.1	169.1	168.8	165.3
C(1)	Ir(1)	C(3)	168.8	177.5	177.3	176.7	176.6
C(1)	Ir(1)	H(1)	91[c]	93.0	93.0	93.3	91.8
C(3)	Ir(1)	H(1)	78[c]	84.5	84.3	83.4	84.7
Ir(1)	Ir(2)	S(1)	55.7	51.8	52.8	50.9	50.8
Ir(1)	Ir(2)	C(2)	161.3	145.5	145.3	145.1	144.7
Ir(1)	Ir(2)	C(3)	49.5	40.1	40.7	42.9	42.2
S(1)	Ir(2)	C(2)	105.7	93.7	92.5	94.2	93.9
S(1)	Ir(2)	C(3)	105.2	91.9	93.5	93.9	93.1
P(2)	Ir(2)	P(4)	161.9	170.6	170.4	167.9	165.9
C(2)	Ir(2)	C(3)	149.1	174.4	174.0	172.0	173.1
Ir(1)	S(1)	Ir(2)	74.3	80.6	70.8	82.0	81.8
Ir(1)	S(1)	O(3)	115.5	120.0	123.6	116.7	117.3
Ir(1)	S(1)	O(4)	115.6	119.9	119.0	116.8	117.3
Ir(2)	S(1)	O(3)	117.0	106.2	109.2	109.0	108.6
Ir(2)	S(1)	O(4)	115.8	106.2	105.3	109.0	108.6
O(3)	S(1)	O(4)	113.3	114.9	115.1	117.0	116.6
Ir(1)	C(1)	O(1)	175.3	175.3	175.7	175.8	175.1
Ir(2)	C(2)	O(2)	177.8	174.4	174.5	173.3	173.6
Ir(1)	C(3)	Ir(2)	82.9	100.7	99.8	95.9	96.9

[a] X-ray structure of **11**. [b] G94 = Gaussian 94. [c] The H(1) position was placed in an idealized position in the X-ray structure.

Table 9. Comparison of Geometries of the Different Calculated Models for Structure **XIa**

(a) Bond Lengths (Å)

atom 1	atom 2	G94[a] B3LYP	G94 (with mod Ir p orb)	Mulliken B3LYP
Ir(1)	Ir(2)	3.06	3.01	3.00
Ir(1)	S(1)	3.29	3.30	3.43
Ir(1)	P(1)	2.40	2.40	2.34
Ir(1)	P(3)	2.40	2.40	2.34
Ir(1)	C(1)	1.85	1.86	1.87
Ir(1)	C(3)	2.30	2.30	2.28
Ir(1)	H(1)	2.07	2.05	2.11
Ir(2)	S(1)	2.62	2.59	2.64
Ir(2)	P(2)	2.42	2.42	2.36
Ir(2)	P(4)	2.42	2.42	2.36
Ir(2)	C(2)	1.88	1.88	1.88
Ir(2)	C(3)	2.31	2.31	2.38
S(1)	O(3)	1.63	1.64	1.48
S(1)	O(4)	1.63	1.64	1.48
O(1)	C(1)	1.18	1.18	1.16
O(2)	C(2)	1.17	1.17	1.16
C(3)	H(1)	1.13	1.14	1.13

(b) Bond Angles

atom 1	atom 2	atom 3	G94[a] B3LYP	G94 (with mod Ir p orb)	Mulliken B3LYP
Ir(2)	Ir(1)	S(1)	48.6	48.1	48.0
Ir(2)	Ir(1)	C(1)	138.1	137.6	134.7
Ir(2)	Ir(1)	C(3)	48.5	49.3	51.4
Ir(2)	Ir(1)	H(1)	77.9	79.0	80.9
S(1)	Ir(1)	C(1)	89.5	89.5	86.8
S(1)	Ir(1)	C(3)	97.1	97.4	99.3
S(1)	Ir(1)	H(1)	126.5	127.1	128.8
P(1)	Ir(1)	P(3)	177.5	177.5	177.3
C(1)	Ir(1)	C(3)	173.4	173.1	173.9
C(1)	Ir(1)	H(1)	144.0	143.4	144.4
C(3)	Ir(1)	H(1)	29.4	29.7	29.5
Ir(1)	Ir(2)	S(1)	70.2	71.7	74.7
Ir(1)	Ir(2)	C(2)	157.2	159.7	163.3
Ir(1)	Ir(2)	C(3)	48.4	48.9	48.5
S(1)	Ir(2)	C(2)	87.0	87.9	88.6
S(1)	Ir(2)	C(3)	118.6	120.7	123.2
P(2)	Ir(2)	P(4)	179.0	177.6	177.7
C(2)	Ir(2)	C(3)	154.4	151.4	148.2
Ir(1)	S(1)	Ir(2)	61.1	60.2	57.4
Ir(1)	S(1)	O(3)	122.2	122.5	121.3
Ir(1)	S(1)	O(4)	122.2	122.1	121.3
Ir(2)	S(1)	O(3)	100.0	100.6	103.8
Ir(2)	S(1)	O(4)	100.0	100.6	103.8
O(3)	S(1)	O(4)	114.3	114.3	117.1
Ir(1)	C(1)	O(1)	179.6	179.6	178.8
Ir(2)	C(2)	O(2)	176.2	176.1	176.7
Ir(1)	C(3)	Ir(2)	83.1	81.8	80.1

[a] G94 = Gaussian 94.

is the C(2)−Ir(2)−C(3) angle, which is computed to be near 175° but is observed at about 150°. One troubling aspect of not including the phenyl groups on the diphosphines in the calculations is the possibility that they may significantly influence the positions of the equatorial ligands through nonbonded contacts. For example, an examination of Figure 5 shows that the phenyl groups are thrust between the equatorial ligands and thus are capable of a significant influence in the positions of these ligands. A further discrepancy between the theoretical models and the X-ray structure lies in the tilt of the SO_2 group with respect to Ir(2). In the X-ray structure the SO_2 group is tilted slightly toward Ir(2) such that the angles between the Ir(1)−S(1) and Ir(2)−S(1) vectors and the SO_2-plane normal are 54.2° and 51.6°. However in the Mulliken calculation, for example, this asymmetry is exaggerated, giving vector-normal angles of 60.8° and 37.4°. We do not currently understand the reasons for the discrepancies between the observed and calculated structural parameters noted above.

Table 10. Selected Bond Lengths and Angles for the Calculated (Mulliken, B3LYP) Structure **XI-TS**

(a) Bond Lengths (Å)

atom 1	atom 2	distance	atom 1	atom 2	distance
Ir(1)	Ir(2)	3.07	Ir(2)	P(4)	2.36
Ir(1)	S(1)	2.57	Ir(2)	C(2)	1.92
Ir(1)	P(1)	2.36	Ir(2)	C(3)	2.09
Ir(1)	P(3)	2.36	S(1)	O(3)	1.48
Ir(1)	C(1)	1.91	S(1)	O(4)	1.48
Ir(1)	C(3)	2.31	O(1)	C(1)	1.15
Ir(1)	H(1)	1.61	O(2)	C(2)	1.16
Ir(2)	P(2)	2.36	C(3)	H(1)	1.94

(b) Bond Angles (deg)

atom 1	atom 2	atom 3	angle	atom 1	atom 2	atom 3	angle
Ir(2)	Ir(1)	S(1)	50.8	S(1)	Ir(2)	C(2)	94.3
Ir(2)	Ir(1)	C(1)	150.2	S(1)	Ir(2)	C(3)	162.8
Ir(2)	Ir(1)	C(3)	42.9	C(2)	Ir(2)	C(3)	162.3
Ir(2)	Ir(1)	H(1)	98.9	Ir(1)	S(1)	Ir(2)	75.1
S(1)	Ir(1)	C(1)	99.4	Ir(1)	S(1)	O(3)	117.1
S(1)	Ir(1)	C(3)	93.7	Ir(1)	S(1)	O(4)	117.1
S(1)	Ir(1)	H(1)	149.7	Ir(2)	S(1)	O(3)	111.7
C(1)	Ir(1)	C(3)	166.9	Ir(2)	S(1)	O(4)	111.7
C(1)	Ir(1)	H(1)	110.9	O(3)	S(1)	O(4)	116.8
C(3)	Ir(1)	H(1)	56.0	Ir(1)	C(1)	O(1)	175.4
Ir(1)	Ir(2)	S(1)	54.0	Ir(2)	C(2)	O(2)	172.8
Ir(1)	Ir(2)	C(2)	148.4	Ir(1)	C(3)	Ir(2)	88.3
Ir(1)	Ir(2)	C(3)	58.8				

In an attempt to gain information about the putative intermediate, immediately preceding the C−H bond activation process that yielded **XIh**, we moved the hydride ligand [within the Ir(1)Ir(2)C(3) plane] to within bonding distance (1.13 Å) of C(3), as found in other complexes containing an asymmetrically bridged methyl group.[57,58] For this structure (**XIa**) we did not complete a Gaussian 94 calculation with S polarization function included in the basis set. Otherwise, the complete range of results on **XIa** is the same as that on **XIh**. Upon convergence of **XIa**, which is only 4.8 kcal/mol higher in energy than **XIh**, a dramatic shortening of the calculated Ir(1)−Ir(2) distance by 0.24 Å occurs, resulting in a distance that is now in line with that observed in the structure of **11**. However, the most dramatic change is in the bonding of the SO_2 ligand, which has moved from an almost symmetrically bridged position in **XIh** to a **terminal** position on Ir(1), leaving it bound in an η^1-pyramidal geometry [Ir(1)−S(1) = 3.43 Å; Ir(2)−S(1) = 2.64 Å]. The resulting geometry at Ir(2), shown in Figure 7b and presented in Table 9, is reminiscent of the SO_2 adduct of Vaska's compound in which the Ir(2)−S(1) distance and the tilt of the SO_2-plane normal to the Ir−S vector (27.2°) are both comparable with the X-ray-derived values (2.49(1) Å and 32(2)°, respectively)[59]; we will comment later about the significance of this calculation.

We have successfully located a transition state (labeled **XI-TS**) relating the two structures **XIh** and **XIa**, at about 4.5 kcal/mol higher in energy than that of **XIa**. The methodology we used to locate this transition state is the same as was described for **III-TS** (see ref 56). The structure of **XI-TS** basically resembles the hydride species **XIh**, as shown in Figure 8c. The major difference in the two can be seen in the hydride position, which is much closer to the methylene group (1.94 vs 2.59 Å) in the transition state. Other important bond lengths and angles are given in Table 10.

(57) Jiménez-Cataño, R.; Hall, M. B. *Organometallics* **1996**, *15*, 1889−1897.
(58) Su, M.-D.; Chu, S.-Y. *J. Am. Chem. Soc.* **1997**, *119*, 5373−5383.
(59) La Placa, S. J.; Ibers, J. A. *Inorg. Chem.* **1966**, *5*, 405.

Scheme 4

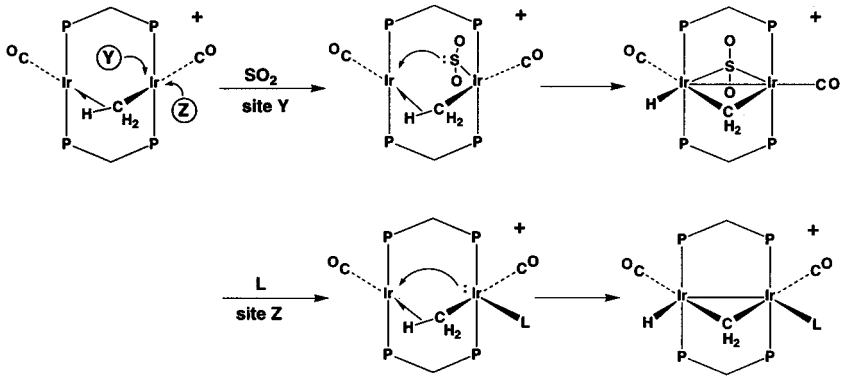

The binding energy of SO_2 in the diiridium complex **11** is calculated as only 4.9 kcal/mol (i.e., the difference between the energies of **IIIt** + SO_2 and **XIh**). Although the other energies resulting from our calculations are consistent with the energy differences obtained from NMR studies, this binding energy seems to be underestimated.

Discussion

As noted earlier, the reactions of the complexes $[MM'(CO)_3(dppm)_2]$ (M, M′ = Rh, Ir) with methyl triflate give rise to three different classes of products, the natures of which are consistent with the different properties of Rh and Ir. Possibly the simplest of these reactions is that involving the mixed Rh/Ir complex, in which simple electrophilic attack at the metals occurs yielding a product in which the methyl group is terminally bound to Ir, presumably reflecting the stronger Ir−C bond. For the dirhodium species the greater tendency for migratory insertion of the lighter congener gives rise to an acyl-bridged product. Reaction of the diiridium complex with methyl triflate is the most novel in this series, having resulted in facile, reversible C−H bond activation of the methyl group, to give $[Ir_2(H)(CO)_3(\mu\text{-}CH_2)(dppm)_2][CF_3SO_3]$ (**2**). Again, the stronger Ir−C and Ir−H bonds, compared with those of Rh, appear to favor the methylene-hydride species in this case.

Although the above-mentioned tricarbonyl species **2** represents our entry point into the chemistry described in this article, the theme of this article is aimed primarily at an investigation of ligand addition to the *dicarbonyl* methyl compound $[Ir_2(CH_3)(CO)_2(dppm)_2][CF_3SO_3]$ (**3**), obtained from **2** through loss of a carbonyl. We have attempted to determine the factors that influence the facile C−H bond cleavage of the methyl group that occurs upon addition of small molecules (CO, PR_3, CNR, and SO_2) to **3**.

Before considering the reactivity of **3**, however, it is instructive to first consider its structure, particularly with regard to the bonding of the methyl group. Two analogous complexes having essentially the same stoichiometry (one having different substituents on the diphosphine and the other having different metals) have been characterized. In the solid state the dirhodium species, $[Rh_2(CH_3)(CO)(\mu\text{-}CO)(dppm)_2]^+$, has a geometry identical with **3**, having a terminal methyl group, whereas the dmpm analogue, $[Ir_2(CO)_2(\mu\text{-}CH_3)(dmpm)_2]^+$, has a symmetrically bridged methyl group. It was clearly of interest to establish whether the different methyl-binding mode in the dmpm species had resulted from the electronic influence of the diphosphine ligands, because the binding mode of the methyl group presumably influences its reactivity. In any case, it seems clear that the different geometries do not differ appreciably in energy, because in solution, compound **3** is fluxional, with the methyl group transferring from metal to metal, presumably via a methyl-bridged intermediate analogous to Kubiak's dmpm-bridged compound. Significantly, the predominant structure of **3** in solution is not that in the solid state; instead the "(μ-CO)-Ir-Me" moiety appears to have twisted so that now both carbonyls and the methyl group are terminally bound. This structure is intermediate between both types of solid-state structures (dppm and dmpm) in which either the carbonyl or the methyl group bridges the metals. DFT calculations on the dhpm analogue of **3** converge to a structure (**IIIt**) which is essentially that proposed in solution (**3a**). Two local minima have been obtained for a methyl-bridged species; the one containing the symmetrically bridged methyl group, exactly analogous to the Kubiak compound, is 0.8 kcal/mol less stable than the unsymmetrically bridged methyl species, in which the methyl group has an agostic interaction with the adjacent metal, and this is in turn ca. 6 kcal/mol less stable than that in which the methyl group is terminally bound (structure **IIIt**). The fluxionality of **3** in solution and the small energy differences obtained from the DFT calculations on the different geometries suggest that the differences observed in the solid state do not reflect electronic stabilization of the different geometries by the two different phosphines, but more likely result from subtle nonbonded contacts in the solid. DFT calculations were also carried out on $[Ir_2H(CO)_2(\mu\text{-}CH_2)(dhpm)_2]^+$ (**IIIh**), the result of cleavage of the agostic C−H interaction in **IIIb** (**agostic**), and a transition state between the two was located. More will be said later about these structures when we discuss the C−H bond-activation process.

In the reactions of **3** with the substrates CO, SO_2, CNR, and PR_3, C−H bond cleavage of the methyl group occurs to yield methylene-bridged hydride structures. Two mechanisms appear possible for this C−H activation process: either C−H activation is induced by ligand addition, or it precedes ligand addition and the resulting methylene-bridged hydride is stabilized by subsequent ligand coordination. Let us begin by considering the former possibility in which ligand attack occurs on complex **3** (or one of its isomers) in which the methyl group is intact. In the reactions of **3**, two basic structural types result in which the added ligand occupies a site in the product either adjacent to (for CO, CNR, or PR_3) or opposite (for SO_2) the bridging methylene unit. This difference is reminiscent of the different sites of attack previously observed in A-frame species, in which SO_2 attack occurred in the A-frame pocket between the metals, whereas other ligands attacked on the outside of the A-frame structure, remote from the adjacent metal.[60] We therefore suggest that ligand attack occurs at either of two sites in an A-frame species such as that shown in Scheme 4 for the agostic, methyl-

(60) (a) Cowie, M. *Inorg. Chem.* **1979**, *18*, 286. (b) Mague, J. T.; Sanger, A. R. *Inorg. Chem.* **1979**, *18*, 2060. (c) George, D. S. A.; McDonald, R.; Cowie, M. *Organometallics* **1998**, *17*, 2553.

bridged structure [structure **IIIb** (**agostic**)]. Under such a scheme ligand attack at site **Y** or **Z** could occur, followed (at some stage) by cleavage of the C−H bond. This proposal is consistent with the DFT calculations that model the *reverse* transformation. In these calculations movement of the hydride ligand in the methylene-bridged hydride product (**XIh**) to give a bridged agostic methyl group also resulted in movement of the SO_2 ligand *away* from the metal at which C−H activation occurred, to a terminal position on the adjacent metal. As noted, the resulting geometry of the SO_2 ligand is pyramidal (as in the SO_2 adduct of Vaska's compound), having the electron lone pair of the pyramidal SO_2 pointed in the direction of the adjacent metal. Presumably, the reverse movement of the SO_2 ligand *toward* the adjacent metal results in donation of the SO_2 lone pair to this metal, resulting in an increase in the electron density at this metal and concomitant C−H bond cleavage of the methyl group. It is significant that under this scheme, initial ligand addition to one metal results in C−H activation at the adjacent metal via transfer of an electron pair from the first metal to the electrophile (SO_2), and subsequent donation of this pair to the second metal. Again, a transition state between the "agostic" intermediate **XIa** and the product of C−H bond cleavage **XIh** has been located at only 4.5 kcal/mol above **XIa** and 9.3 kcal/mol above **XIh**. It is encouraging that these energy differences are in line with the very low barrier of 6.1 kcal/mol obtained from NMR studies (vide supra).

When ligand attack is on the outside of the A-frame complex **IIIb** (**agostic**) (site **Z** in Scheme 4), as with phosphines and isocyanides, this electronic influence must be transmitted to the second metal via the metal−metal framework, because the added ligand is not in a position to interact directly with this adjacent metal. In this case we propose that addition at site **Z** gives an 18e center which can result in formation of a dative Ir → Ir bond, which supplies the additional electron density at the adjacent metal, leading to C−H bond cleavage.

As in other A-frame complexes, we assume that CO attack occurs at the outside site (**Z**), much as for PR_3 and CNR groups. Irrespective of site of attack, however, the net result of attack at one metal is C−H bond cleavage by the other metal. The major difference in attack at site **Y** or **Z** is whether the electronic effect of ligand coordination at one metal is transmitted to the adjacent metal via the attacking ligand, which assumes a bridging coordination mode, or via a direct metal−metal interaction. In this scheme the preference of SO_2 for site **Y** is presumably thermodynamic, resulting from the preference of the electrophile to access the electron density of both metals and therefore be in the bridging site, whereas the preference of other ligands for site **Z** is assumed to be kinetic, having less steric repulsions in this site at one end of the complex.

An alternate mechanism for methyl-group activation involves C−H bond cleavage in the precursor **3**, *before* ligand attack, to give small, undetectable concentrations of an intermediate such as **IIIh** (Figure 7). The final products of ligand attack on this intermediate would result from coordination at a vacant site on the adjacent metal. The same factors discussed earlier would favor SO_2 attack at the inside site, leading to a bridging mode, whereas the other ligands would favor attack at the less sterically encumbered external site. Certainly the energy of this intermediate (**IIIh**) is calculated as only 3.4 kcal/mol less stable than that of the agostically bound **IIIb**, therefore it is accessible. However, there are two aspects of this study that lead us to favor the first mechanism of C−H bond cleavage over the second; i.e., C−H bond cleavage induced by ligand addition, rather than before ligand addition. First, in the calculations performed, the activation barrier to C−H cleavage [starting from the agostic structures **IIIb (agostic)** and **XIb**] is substantially less with SO_2 coordinated than without (ca. 5 vs 15 kcal/mol), indicating that this process is favored by SO_2 addition. Second, the experimental NMR evidence of facile and reversible exchange of the methylene hydrogens and the hydride ligand in the CO (**2**) and SO_2 (**11**) adducts demonstrates that reversible C−H bond cleavage/formation is occurring in these adducts and therefore argues strongly for the second mechanism.

Conclusions

Facile C−H bond cleavage of the methyl group in $[Ir_2(CH_3)(CO)_2(dppm)_2]^+$ occurs upon addition of several small molecules such as CO, CN^tBu, phosphines, triphenyl phosphite, and SO_2, yielding either $[Ir_2H(CO)_2L(\mu\text{-}CH_2)(dppm)_2]^+$ (L = CO, CN^t-Bu, PR_3) or $[IrH(CO)_2(\mu\text{-}CH_2)(\mu\text{-}SO_2)(dppm)_2]^+$. Although C−H activation has been observed previously upon addition of phosphines,[45] it has not, to our knowledge, been observed upon addition of strong π-acid ligands such as CO and SO_2. In all cases reported herein, we propose that C−H bond cleavage at one metal results from ligand binding at the *adjacent* metal. In this regard, SO_2 is unique in this study. It functions first as an electrophile and subsequently as a nucleophile, acting as an electron conduit, accepting an electron pair from one metal and passing it on to the adjacent metal. The resulting electron density increase at the second metal presumably results in C−H bond cleavage by donation into the antibonding orbital of the C−H bond that is involved in an agostic interaction with the adjacent metal. For other ligands the metal at which addition occurs attains an 18-valence electron count leading to dative metal−metal bond formation to the adjacent metal. It is this dative bond that supplies the necessary electron density to cleave the C−H bond. We are unaware of any other system in which such metal−metal cooperativity effects result in C−H bond activation.

This study has also demonstrated that the activation barrier to methyl group C−H bond cleavage can be unusually low in these binuclear systems. The value observed for interconversion between methyl and methylene groups ($\Delta H^{\ddagger} = 6$ kcal/mol) in the SO_2 adduct, $[Ir_2H(CO)_2(\mu\text{-}CH_2)(\mu\text{-}SO_2)(dppm)_2][CF_3SO_3]$, is in fact very close to values of between 6 and 8 kcal/mol observed for platinum-surface−bound alkyls.[61] This supports our contention that binuclear complexes can function as useful models for adjacent-metal involvement in heterogeneous systems. As stated by Fehlner and co-workers,[62] "...reaction paths depend on small energy differences that can induce large changes in rates...if one wants to model catalytic reactivity with cluster chemistry, small barrier processes must be understood." In this study we have developed an improved understanding of the function of the adjacent metals in the facile and reversible C−H bond cleavage process of a methyl group.

Acknowledgment. We thank the Natural Sciences and Engineering Research Council of Canada (NSERC) and the University of Alberta for financial support of the research and for scholarships (to J.R.T.), and NSERC for funding the P4/RA diffractometer. The Calvin College contingent wishes to thank the college for a sabbatical leave to RDK, the donors of the Petroleum Research Fund, administered by the American Chemical Society, and the Camille and Henry Dreyfus Foundation for a Scholar/Fellow award to undergraduate institutions.

(61) Zaera, F. *Acc. Chem. Res.* **1992**, *25*, 260.

(62) Dutta, T. K.; Vites, J. C.; Jacobsen, G. B.; Fehlner, T. P. *Organometallics* **1987**, *6*, 842.

We also thank Dr. R. E. D. McClung and G. Aarts for assistance with the NMR saturation transfer experiments and the line-shape analysis on compounds **2** and **11**, respectively, and Dr. McClung for many helpful discussions.

Supporting Information Available: Listings of crystal data, data collection, solution and refinement, complete atomic coordinates, bond distances and angles, and thermal parameters for compounds **3**, **6** and **11**, Tables of atom coordinates from DFT calculations for structures **IIIt**, **IIIb (agostic)**, **IIIb (symmetric)**, **IIIh**, **III-TS**, **XIh**, **XIa**, and **XI-TS**. This material is available free of charge via the Internet at http://pubs.acs.org.

JA983525O